

# Modeling and simulation of nonlinear electro-thermo-mechanical continua with application to shape memory polymeric medical devices

Innocent Niyonzima<sup>a</sup>, Yang Jiao<sup>a</sup>, Jacob Fish<sup>a</sup>

<sup>a</sup>*Columbia University, Department of Civil Engineering and Engineering Mechanics, New York, 10027 NY, USA.*

---

## Abstract

Shape memory materials have gained considerable attention thanks to their ability to change physical properties when subjected to external stimuli such as temperature, pH, humidity, electromagnetic fields, etc. These materials are increasingly used for a large number of biomedical applications. For applications inside the human body, contactless control can be achieved by the addition of electric and/or magnetic particles that can react to electromagnetic fields, thus leading to a composite biomaterial. The difficulty of developing accurate numerical models for smart materials results from their multiscale nature and from the multiphysics coupling of involved phenomena. This coupling involves electromagnetic, thermal and mechanical problems. This paper contributes to the multiphysics modeling of a shape memory polymer material used as a medical stent. The stent is excited by electromagnetic fields produced by a coil which can be wrapped around a failing organ. In this paper we develop large deformation formulations for the coupled electro-thermo-mechanical problem using the electric potential to solve the electric problem. The formulations are then discretized and solved using the finite element method. Results are validated by comparison with results in the literature.

**Keywords:** Multiphysics modeling, electro-thermo-mechanical coupling, shape memory polymers stents, large deformations.

**2010 MSC:** 34A34, 34A36, 34A37, 65L20

---

## 1. Introduction

The increase of life expectancy creates a need to maintain the functions of aging organs to allow greater independence for the elderly. Biomaterial implants have the potential to fulfill some of these functions. The total number of implants in the world exceeds four hundred million per year and grows every year [1]. Biomaterials are also increasingly used for a large number of biomedical applications such as the prevention and cure of coronary heart disease and stroke, as well as ophthalmological applications, biosensors and drug delivery systems [2, 3]. They have the potential to contribute to the reduction of the cost of health and the improvement of the life conditions.

Among biomaterials, shape memory materials have gained considerable attention in the biomedical community thanks to their ability to change physical properties (morphing, structural rigidity, refractive index, etc.) when subjected to external stimuli such as temperature, pH, humidity, electromagnetic fields, etc. This special behavior results from the the shape memory effect observed in shape memory materials [4]. They are used in minimally invasive surgery as embolic devices to treat aneurysm [5, 6] and as vascular stents [7, 8, 9]. Figure 1 illustrate the deployment of a stent in a blood vessel. They can also be used as portable sensors to monitor heart and respiratory rates and in controlled drug delivery systems thus allowing to reduce the side effects of drugs [11, 12]. For these different uses, biomaterials must possess a number of properties. They must be biocompatible to avoid toxicity in contact with biological tissues. Biodegradability is a desirable property for temporary implants, and for minimally invasive in vivo surgery applications, devices must be controllable without contact and self-expanding. All of these properties make polymers the best candidates for a wide range of biomedical applications. Contactless control can be achieved by the addition of electric/magnetic (nano)particles inclusions to produce a smart composite that can react to electromagnetic fields.

Accurate numerical models for smart composites must account for the multiphysics coupling which involve different domains of physics (electromagnetism,

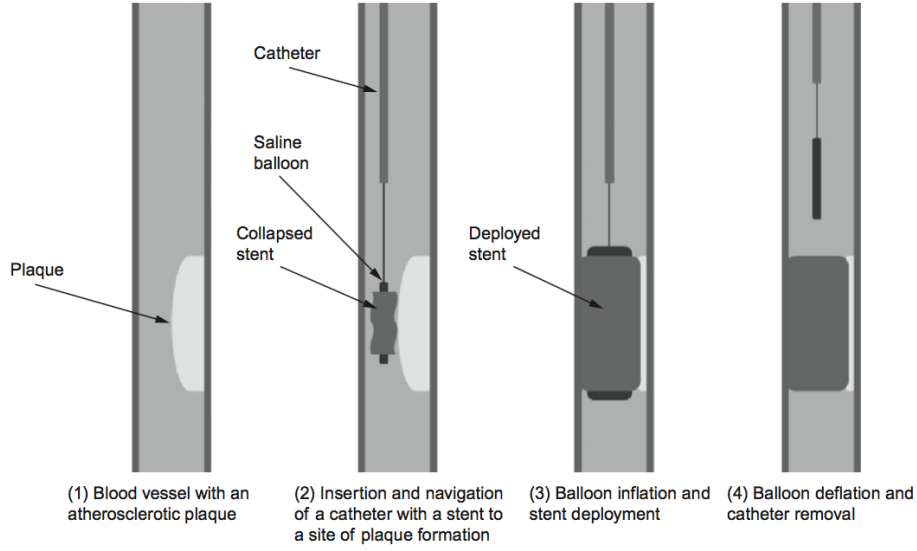


Figure 1: Diagram illustrating the deployment of a stent in a blood vessel [10].

31 thermal, mechanics) and the multiscale nature of the materials. The present  
 32 manuscript is concerned with multiphysics modeling of shape memory polymer  
 33 materials used for biomedical devices for homogeneous materials. The difficulty  
 34 of developing multiphysics models arises from a number of factors. (a) The  
 35 *geometric non-linearity* resulting from large mechanical deformations leads to  
 36 the modification of the equations that govern the electromagnetic and thermal  
 37 problems to account for motion. Additional complexity for the electromagnetic  
 38 problem results from the presence of electromagnetic fields in the air and vac-  
 39 uum. (b) The *material non-linearities* resulting from the presence of materials  
 40 with nonlinear thermal constitutive laws, plastic and viscous laws for mechanics  
 41 and nonlinear anhysteretic/hysteretic constitutive laws for electromagnetism.

42 Models and numerical simulations have already been developed for mul-  
 43 tiphysics problems in piezoelectric, magnetostrictive, and piezomagnetic ma-  
 44 terials in the case of small deformations [13, 14, 15, 16, 17, 18, 19]. The-  
 45 oretical models have also been developed for thermomechanical and electro-  
 46 magneto-thermomechanical problems in the case of large mechanical deforma-

47 tions [20, 21, 22, 23]. Popular numerical implementations combine the La-  
 48 grangian approach for the mechanical problem and the Eulerian or arbitrary  
 49 Lagrangian Eulerian approach for the electromagnetic problem [24, 25]. In  
 50 this paper we consider low frequency electromagnetic problems and solve for a  
 51 scalar potential formulation only defined in the mechanical domain. Thus, a  
 52 Lagrangian mesh can also be used for the electromagnetic problem.

53 The development of multiphysics models for smart composites controlled by  
 54 electromagnetic fields is still in its infancy. Electro-magneto-mechanical mod-  
 55 els using electrostatic and magnostatic formulations have been developed for  
 56 magneto-sensitive composites and magneto-electro-elastic composites (e.g., elec-  
 57 tro active polymers ) in large deformations [26, 27, 28]. In [29], the discontinuous  
 58 Galerkin method was used to solve the electro-thermo-mechanical problem in  
 59 a SMP by solving an electrokinetic problem excited by surface currents. For a  
 60 more effective contactless control, the multiphysics problem should include eddy  
 61 currents and hysteretic losses as a means of controlling the temperature.

62 In this paper, we develop a simple multiphysics model for an electromag-  
 63 netically controlled vascular stent excited by a coil. The paper extends the  
 64 thermomechanical model developed in [30] by proposing a contactless electro-  
 65 magnetic control of the temperature, especially during the recovery step that  
 66 takes place inside the human body. For the sake of clarity and in order to have a  
 67 self-sufficient paper which is easily accessible by the mechanics and electromag-  
 68 netic communities, we derive the general fully coupled problem from Maxwell  
 69 equations and conservation laws using the Lagrangian and Eulerian formalisms.  
 70 Then, a simplified, quasistatic electro-thermo-mechanical problem is derived  
 71 and discretized using the finite element (FE) method.

72 The paper is organized as follows: in Section 2 we recall Maxwell's equations  
 73 and conservation laws using the Lagrangian and the Eulerian formalisms. In Sec-  
 74 tion 3, we derive the simplified coupled problem and its strong and weak forms  
 75 using potential formulations. The weak formulations are then semi-discretized  
 76 in space using the FE method and in time using the backward Euler time step-  
 77 ping method. The resulting system of nonlinear algebraic equations is linearized

78 and solved using the Newton–Raphson method. Section 4 deals with numeri-  
79 cal examples. At first, we validate the thermo-mechanical formulation for SMP  
80 materials with simple geometries along the lines of [30]. We then study the  
81 behavior of the electromagnetically responsive SMP stent excited by a coil. In  
82 Section 5 we close the paper with conclusions and perspectives.

## 83 2. Governing equations of the general multiphysics problem

84 In this section, the general electro-magneto-thermo-mechanical coupled prob-  
85 lem is derived from Maxwell’s equations and conservation laws. Throughout the  
86 paper, we use the indices  $E$  and  $L$  to denote the Eulerian and Lagrangian quan-  
87 tities. Thus,  $\mathbf{f}_E$  and  $\mathbf{f}_L$  denote the forces in the Eulerian and Lagrangian  
88 framework, respectively. The open domains  $\Omega_0^{\text{Mec}}$ ,  $\Omega_0^{\text{The}}$  and  $\Omega_0^{\text{Ele}}$  denote the  
89 undeformed computational domains for the mechanical, thermal and electro-  
90 magnetic problems, respectively. Likewise,  $\Omega_t^{\text{Mec}}$ ,  $\Omega_t^{\text{The}}$  and  $\Omega_t^{\text{Ele}}$  denote the  
91 deformed computational domains for the mechanical, thermal and electromag-  
92 netic problems at a time  $t \in \mathcal{I}_t := ]t_0, t_{\text{end}}[$ . The domains of the mechanical and  
93 thermal problems are generally subdomains of the electromagnetic domain, i.e.,  
94  $\Omega_i^{\text{Mec}} \subseteq \Omega_i^{\text{Ele}}$  and  $\Omega_i^{\text{The}} \subseteq \Omega_i^{\text{Ele}}$  with  $i = \{0, t\}$  as the electromagnetic fields can  
95 be defined in the entire domain including the surrounding air. The domains  
96  $\Omega_{c,i} \subseteq \Omega_i^{\text{Ele}}$ ,  $\Omega_{c,i}^C \subseteq \Omega_i^{\text{Ele}}$  and  $\Omega_{s,i} \subsetneq \Omega_{c,i}^C \subset \Omega_i^{\text{Ele}}$  are the conductors, non-  
97 conductors and inductors where the electric currents source is imposed. The  
98 domains  $\Gamma_i^{\text{Ele}}$ ,  $\Gamma_i^{\text{The}}$  and  $\Gamma_i^{\text{Mec}}$  denote the boundaries of the electromagnetic, ther-  
99 mal and mechanical domains, respectively. The differential operators **Grad**,  
100 **Curl** and **Div** denote the gradient, rotational and divergence operators defined  
101 on the undeformed configurations while *grad*, *curl* and *div* denote the same  
102 operators defined on the deformed configurations.

### 103 2.1. Kinematics

The motion is described by the mappings  $\varphi_t$  and  $\varphi$  assumed to be smooth  
enough (we do not consider fracture). The mapping  $\varphi_t$  is also assumed to be

bijjective and defined by:

$$\begin{aligned}\varphi_t : \Omega_0^{\text{Mec}} &\rightarrow \mathbb{E}^3, \\ \mathbf{X} &\mapsto \mathbf{x} = \varphi_t(\mathbf{X}) = \varphi(\mathbf{X}, t) = \mathbf{X} + \mathbf{u}(\mathbf{X}, t)\end{aligned}\tag{2.1}$$

where  $\mathbf{X}$  is the position of a particle point P in the undeformed configuration,  $\mathbf{x}$  is the position of P in the deformed configuration,  $\mathbf{u}$  is the vector of displacements and  $\mathbb{E}^3$  is the three dimensional Euclidean space [31]. The positions in the undeformed and deformed configurations are related by  $\mathbf{X} = \varphi_t^{-1}(\mathbf{x})$  which is valid thanks to the bijection of  $\varphi_t$ . For any time  $t \in \mathcal{I}_t$ , the deformed configurations are also defined as:

$$\Omega_t^{\text{Mec}} := \varphi_t(\Omega_0^{\text{Mec}}), \quad \Omega_t^{\text{The}} := \varphi_t(\Omega_0^{\text{The}}), \quad \Omega_t^{\text{Ele}} := \varphi_t(\Omega_0^{\text{Ele}}).\tag{2.2}$$

The deformation gradient tensor and its determinant are given by:

$$\mathbf{F} := \frac{\partial \mathbf{x}}{\partial \mathbf{X}} = \mathbf{Grad} \varphi = \mathbb{1} + \mathbf{Grad} \mathbf{u} \quad , \quad J = \det \mathbf{F}\tag{2.3}$$

where  $\mathbb{1}$  is the identity matrix. The velocity  $\mathbf{v}$  and acceleration  $\mathbf{a}$  are given by:

$$\mathbf{v}(\mathbf{X}, t) = \frac{\partial \varphi}{\partial t}(\mathbf{X}, t), \quad \mathbf{a}(\mathbf{X}, t) = \frac{\partial \mathbf{v}}{\partial t}(\mathbf{X}, t) = \frac{\partial^2 \varphi}{\partial t^2}(\mathbf{X}, t).\tag{2.4}$$

Assuming the existence of a mapping  $\Theta$ :

$$\begin{aligned}\Theta : \mathbb{E}^3 \times \mathcal{I}_t &\rightarrow \Omega_0^{\text{Mec}} \subsetneq \mathbb{E}^3, \\ (\mathbf{x}, t) &\mapsto \mathbf{X} = \Theta(\mathbf{x}, t) = \Theta(\varphi(\mathbf{X}, t), t),\end{aligned}\tag{2.5}$$

it is possible to derive the following relationship:

$$\frac{D\mathbf{X}}{Dt} = \frac{\partial \Theta}{\partial \varphi} \frac{\partial \varphi}{\partial t} + \frac{\partial \Theta}{\partial t} = \mathbf{F}^{-1} \mathbf{v} + \mathbf{V} = \mathbf{0},\tag{2.6}$$

which relates the *matter flow field*  $\mathbf{V}$  to the velocity  $\mathbf{v}$  as:

$$\mathbf{V} = -\mathbf{F}^{-1} \mathbf{v}.\tag{2.7}$$

104 The matter flow field is important for the definition of the electromagnetic prob-  
105 lem on the undeformed configuration. The independence of the initial position  
106  $\mathbf{X}$  on the time was used to derive (2.6).

107 *2.2. Maxwell's equations*

108 We recall non-relativistic Maxwell's equations on moving domains under  
109 large deformations, using Eulerian and Lagrangian formalisms [32, 33, 21, 20].

110 *2.2.1. Full Maxwell's equations in Eulerian formalism*

In Eulerian setting, the electromagnetic fields are governed by the following Maxwell's equations [34, 20]:

$$\mathbf{curl} \mathbf{h} = \mathbf{j} + \partial_t \mathbf{d}, \quad \mathbf{curl} \mathbf{e} = -\partial_t \mathbf{b}, \quad \operatorname{div} \mathbf{b} = 0, \quad \operatorname{div} \mathbf{d} = \rho_E, \quad (2.8 \text{ a-d})$$

and constitutive laws:

$$\begin{aligned} \mathbf{h} &= \mu_0^{-1} \mathbf{b} - \underbrace{(\mathbf{m} - \mathbf{v} \times \mathbf{p})}_{\mathbf{m}_{\text{eff}}} = \boldsymbol{\nu}_E(\mathbf{b}) \mathbf{b} + \mathbf{v} \times \mathbf{p} = \mathbf{H}(\mathbf{e}, \mathbf{b}, \mathbf{v}), \\ \mathbf{d} &= \epsilon_0 \mathbf{e} + \mathbf{p} = \epsilon_0 \epsilon_{rE}(\mathbf{e}) \mathbf{e} = \boldsymbol{\epsilon}_E(\mathbf{e}) \mathbf{e} = \mathbf{D}(\mathbf{e}), \\ \mathbf{j} &= \boldsymbol{\sigma}_E(\underbrace{\mathbf{e} + \mathbf{v} \times \mathbf{b}}_{\mathbf{e}_{\text{eff}}}) + \mathbf{j}_s + \rho_E \mathbf{v} = \mathbf{j}_{\text{eff}} + \rho_E \mathbf{v} = \mathbf{J}(\mathbf{e}, \mathbf{b}, \mathbf{v}). \end{aligned} \quad (2.9 \text{ a-c})$$

In (2.8 a-d)–(2.9 a-c),  $\mathbf{h}$  is the magnetic field (A/m),  $\mathbf{b}$  the magnetic flux density (T),  $\mathbf{j}$  the electric current density (A/m<sup>2</sup>),  $\mathbf{d}$  the electric flux density (C/m<sup>2</sup>),  $\mathbf{e}$  the electric field (V/m) and  $\rho_E$  the electric charge density (C/m<sup>3</sup>). The fields  $\mathbf{e}_{\text{eff}}$  and  $\mathbf{j}_{\text{eff}}$  are the effective electric field and effective electric current density, whereas  $\mathbf{j}_s$  (A/m<sup>2</sup>) is the electric current source defined in the inductors  $\Omega_{s,t}$  and  $\boldsymbol{\sigma}_E$  is the electric conductivity tensor ( $\Omega/\text{m}$ ). The magnetization  $\mathbf{m}$  (A/m) and polarization  $\mathbf{p}$  (C/m<sup>2</sup>) are defined by:

$$\mathbf{m} = \mu_0^{-1} \boldsymbol{\chi}_{bE}(\mathbf{b}) \mathbf{b}, \quad \mathbf{p} = \epsilon_0 \boldsymbol{\chi}_{eE}(\mathbf{e}) \mathbf{e} = \frac{\boldsymbol{\chi}_{eE}}{\mathbb{1} + \boldsymbol{\chi}_{eE}} \mathbf{d}, \quad (2.10 \text{ a-b})$$

111 where  $\boldsymbol{\chi}_{bE}$  and  $\boldsymbol{\chi}_{eE}$  are the magnetic and electric susceptibility tensors,  $\mu_0 =$   
112  $4\pi 10^{-7}$  is the magnetic permeability of the free space (H/m) and  $\epsilon_0 \simeq 10^{-9}/36\pi$   
113 is the electric permittivity of the free space (C<sup>2</sup>/Nm<sup>2</sup>). Another definition of  
114 magnetic susceptibility  $\boldsymbol{\chi}_{mE}$  with  $\mathbf{m} = \boldsymbol{\chi}_{mE} \mathbf{h}$  is often used in the constitu-  
115 tive law dual to (2.10 a). Additionally,  $\boldsymbol{\nu}_E = \mu_0^{-1}(\mathbb{1} - \boldsymbol{\chi}_{bE})$  is the magnetic  
116 reluctivity tensor,  $\boldsymbol{\mu}_E = \boldsymbol{\nu}_E^{-1}$  is the magnetic permeability tensor,  $\boldsymbol{\epsilon}_E$  is the

117 electric susceptibility tensor,  $\epsilon_{rE}(\mathbf{e})$  is the relative electric permittivity tensor  
 118 with  $\epsilon_{rE}(\mathbf{e}) = \mathbf{1} + \chi_{eE}(\mathbf{e})$  and  $\mathbf{v}$  is the velocity (m/s). The dependency of the  
 119 mapping  $\mathbf{H}$  on (2.9 a) on the electric field  $\mathbf{e}$  results from (2.10 b). The motion  
 120 is accounted for by the velocity terms in the constitutive laws (2.9 a-c).

### 121 2.2.2. Full Maxwell's equations in Lagrangian formalism

In Lagrangian setting, the electromagnetic fields are governed by the following Maxwell's equations (see [32, 33, 21, 20, 23] and [35, Appendix F]):

$$\mathbf{Curl} \mathcal{H}_{\text{eff}} = \mathcal{J} + \partial_t \mathcal{D}, \quad \mathbf{Curl} \mathcal{E}_{\text{eff}} = -\partial_t \mathcal{B}, \quad \text{Div} \mathcal{B} = 0, \quad \text{Div} \mathcal{D} = \rho_L, \quad (2.11 \text{ a-d})$$

and constitutive laws:

$$\mathcal{H}_{\text{eff}} = \underbrace{J^{-1} \mathbf{F}^T (\nu_E \circ \varphi_t^{-1}) \mathbf{F} \mathcal{B}}_{\nu_L} + (\epsilon_{rE} \circ \varphi_t^{-1})^{-1} (\mathbf{V} \times \mathcal{D}) \quad (2.12)$$

$$\mathcal{D} = \underbrace{J \mathbf{F}^{-1} (\epsilon_E \circ \varphi_t^{-1}) \mathbf{F}^{-T}}_{\epsilon_L} (\underbrace{\mathcal{E}_{\text{eff}} + \mathbf{V} \times \mathcal{B}}_{\mathcal{E}}), \quad (2.13)$$

$$\mathcal{J} = \underbrace{J \mathbf{F}^{-1} (\sigma_E \circ \varphi_t^{-1}) \mathbf{F}^{-T}}_{\sigma_L} \mathcal{E}_{\text{eff}} + \mathcal{J}_s \quad (2.14)$$

122 defined on the undeformed configuration  $\Omega_0^{\text{Ele}}$ . In (2.11 a-d) and (2.12)–(2.14),  
 123  $\mathcal{H}$  is the magnetic field (A/m),  $\mathcal{B}$  the magnetic flux density (T),  $\mathcal{J}$  the electric  
 124 current density (A/m<sup>2</sup>),  $\mathcal{D}$  the electric flux density (C/m<sup>2</sup>),  $\mathcal{E}_{\text{eff}}$  the effective  
 125 electric field,  $\mathcal{E}$  the electric field (V/m),  $\mathcal{J}_s$  (A/m<sup>2</sup>) the current source defined  
 126 in the inductors  $\Omega_{s,0}$  and  $\mathbf{V}$  is the matter flow field (m/s) defined in (2.6). The  
 127 tensor  $\sigma_L$  is the electric conductivity tensor (Ω/m) and  $\rho_L$  is the electric charge  
 128 density (C/m<sup>3</sup>). The notation  $(\mathbf{f} \circ \varphi_t^{-1})(\mathbf{x}) := \mathbf{f}(\varphi_t^{-1}(\mathbf{x}))$  is used.

The one differential forms are transformed as:

$$\begin{aligned} \mathcal{H}_{\text{eff}} &= \mathbf{F}^T (\mathbf{h} - \mathbf{v} \times \mathbf{d}), \quad \mathcal{E}_{\text{eff}} = \mathbf{F}^T (\mathbf{e} + \mathbf{v} \times \mathbf{b}), \\ \mathcal{E} &= \mathcal{E}_{\text{eff}} + \mathbf{V} \times \mathcal{B} = \mathbf{F}^T \mathbf{e}. \end{aligned} \quad (2.15 \text{ a-c})$$

and the two differential forms are transformed as:

$$\mathcal{B} = J \mathbf{F}^{-1} \mathbf{b}, \quad \mathcal{D} = J \mathbf{F}^{-1} \mathbf{d}, \quad \mathcal{J} = J \mathbf{F}^{-1} \mathbf{j}, \quad \mathcal{J}_s = J \mathbf{F}^{-1} \mathbf{j}_s. \quad (2.16)$$



In (2.15 c),  $\mathbf{V} \times \mathbf{B} = -\mathbf{F}^T(\mathbf{v} \times \mathbf{b})$  results from the identity:

$$\mathbf{F}^T \mathbf{v} \times \mathbf{F}^T \mathbf{b} = J \mathbf{F}^{-1}(\mathbf{v} \times \mathbf{b}), \quad (2.17)$$

129 which is valid for any matrix  $\mathbf{F} \in GL_3(\mathbb{R})$  [35, Formula B.11].

Additionally, the magnetization  $\mathcal{M}$  is related to the magnetic induction by:

$$\begin{aligned} \mathcal{M} &= \mathbf{F}^T \mathbf{m} = \mathbf{F}^T(\mu_0^{-1} \chi_{bE} \mathbf{b}) = \mathbf{F}^T(\mu_0^{-1} \chi_{bE} J^{-1} \mathbf{F} \mathbf{B}) \\ &= \mu_0^{-1} J^{-1} \mathbf{F}^T \chi_{bE} \mathbf{F} \mathbf{B} = \mu_0^{-1} \chi_{bL} \mathbf{B} = (\mu_0^{-1} \mathbb{1} - \nu_L) \mathbf{B}, \end{aligned} \quad (2.18)$$

while the effective magnetization  $\mathcal{M}_{\text{eff}}$  is given by:

$$\mathcal{M}_{\text{eff}} = \mathbf{F}^T(\mathbf{m} - \mathbf{v} \times \mathbf{p}) = \mathcal{M} + \mathbf{V} \times \mathcal{P}, = (\mu_0^{-1} \mathbb{1} - \nu_L) \mathbf{B} + \mathbf{V} \times \mathcal{P} \quad (2.19)$$

where the polarization is related to the electric flux density by [35]:

$$\mathcal{P} = \frac{\epsilon_{rL} - \mathbb{1}}{\epsilon_{rL}} \mathcal{D} = \frac{\chi_{eE}}{\mathbb{1} + \chi_{eE}} \mathcal{D}. \quad (2.20)$$

Combining all these results, the following transformations for second order tensors used in constitutive laws can be derived:

$$\begin{aligned} \nu_L &= J^{-1} \mathbf{F}^T \nu_E \mathbf{F}, \mu_L = J \mathbf{F}^{-1} \mu_E \mathbf{F}^{-T}, \\ \epsilon_L &= J \mathbf{F}^{-1} \epsilon_E \mathbf{F}^{-T}, \sigma_L = J \mathbf{F}^{-1} \sigma_E \mathbf{F}^{-T}. \end{aligned} \quad (2.21)$$

### 130 2.3. Conservation equations

131 We recall conservation equations using the Eulerian and Lagrangian for-  
132 malisms.

#### 133 2.3.1. Conservation equations using the Eulerian description

In Eulerian setting, the conservation equations read [36, 31, 37]:

$$\frac{D\rho}{Dt} + \rho \operatorname{div} \mathbf{v} = 0, \quad \rho \frac{D\mathbf{v}}{Dt} - \operatorname{div} \boldsymbol{\sigma} = \mathbf{f}_E, \quad \epsilon_P : \boldsymbol{\sigma} + \mathbf{L}_E = 0. \quad (2.22 \text{ a-c})$$

$$\rho \frac{DU_E}{Dt} + \operatorname{div} \mathbf{q}_E = \boldsymbol{\sigma} : \mathbf{L} + w_E. \quad (2.23)$$

Equations (2.22 a-c) are balance equations of the mass, linear and angular momentum and (2.23) is the balance equation of the internal energy. The quantity  $\rho$  is the mass density ( $\text{kg m}^{-3}$ ),  $\boldsymbol{\sigma}$  is the Cauchy stress ( $\text{N/m}^2$ ),  $\mathbf{f}_E$  is the volume force ( $\text{N/m}^3$ ),  $\epsilon_P$  is the third order permutation tensor also known as the Levi Civita tensor such that  $(\epsilon_P \boldsymbol{\sigma})_i = (\epsilon_P)_{ijk} \sigma_{jk}$ ,  $\mathbf{L}_E$  is the torque,  $U_E$  is the density of internal energy,  $\mathbf{q}_E$  is the heat flux density,  $\mathbf{L} := \mathbf{grad} \mathbf{v}$  is the gradient deformation and  $w_E$  is the electromagnetic source term for the heat problem.

The electromagnetic force, torque, internal energy and source term are given by:

$$\begin{aligned} \mathbf{f}_E = \rho_E \mathbf{e} + \mathbf{j} \times \mathbf{b} + (\mathbf{grad} \mathbf{e})^T \mathbf{p} + (\mathbf{grad} \mathbf{b})^T \mathbf{m} \\ + \partial_t (\mathbf{p} \times \mathbf{b}) + \text{div} [\mathbf{v} \otimes (\mathbf{p} \times \mathbf{b})], \end{aligned} \quad (2.24)$$

$$\mathbf{L}_E = \mathbf{p} \times \mathbf{e} + (\mathbf{m} - \mathbf{v} \times \mathbf{p}) \times \mathbf{b}, \quad (2.25)$$

$$\rho \frac{DU_E}{Dt} = \rho c_p \frac{\partial \vartheta_E}{\partial t}, \quad (2.26)$$

$$w_E = \mathbf{j}_{\text{eff}} \cdot \mathbf{e}_{\text{eff}} - \mathbf{m}_{\text{eff}} \cdot \frac{\partial \mathbf{b}}{\partial t} + \rho \frac{\partial}{\partial t} \left( \frac{\mathbf{p}}{\rho} \right) \cdot \mathbf{e}_{\text{eff}} \quad (2.27)$$

where  $c_p$  and  $\vartheta_E$  are the heat capacity and the temperature, respectively. Equations (2.22 c) and (2.25) suggest that Cauchy stress  $\boldsymbol{\sigma}$  may not be symmetric in presence of electromagnetic fields. However, symmetry may be kept for isotropic materials.

Equations (2.22)–(2.23) must be completed by constitutive laws derived from the *Clausius-Duhem inequality*. In this paper, we assume the following nonlinear constitutive law for the thermal problem [37]:

$$\mathbf{q}_E = \mathbf{Q}(\vartheta_E, \mathbf{grad} \vartheta_E) = -\boldsymbol{\kappa}_E(\vartheta_E) \mathbf{grad} \vartheta_E \quad (2.28)$$

where  $\boldsymbol{\kappa}_E$  is the thermal conductivity tensor ( $\text{W/mK}$ ). The thermo-mechanical constitutive law involves the definition of an appropriate objective rate  $\boldsymbol{\sigma}^\nabla$  (e.g., Jaumann rate, Truesdell rate or Green-Naghdi rate) which is related to the material derivative of the Cauchy stress  $\dot{\boldsymbol{\sigma}}$  [37] as:

$$\boldsymbol{\sigma}^\nabla = \dot{\boldsymbol{\sigma}} - \boldsymbol{\psi}(\mathbf{L}, \mathbf{F}) = \boldsymbol{\Sigma}(\boldsymbol{\sigma}, \mathbf{L}, \mathbf{F}, \vartheta_E, \mathbf{Z}_E(\tau \leq t)), \quad \mathbf{L} = \dot{\mathbf{F}} \mathbf{F}^{-1} \quad (2.29 \text{ a-b})$$

145 where the velocity gradient  $\mathbf{L}$  is related to the rate of the deformation gradient  
 146  $\dot{\mathbf{F}}$  through (2.29 b) and  $\mathbf{Z}_E(\tau \leq t)$  is the set of internal variables that account  
 147 for the history of the loadings.

### 148 2.3.2. Conservation equations using the Lagrangian description

In Lagrangian setting, the conservation equations read [36, 31, 37]:

$$\rho_0 - \rho J = 0, \quad \rho_0 \frac{D^2 \mathbf{u}}{Dt^2} - \text{Div } \mathbf{F} \mathbf{S} = \mathbf{f}_L, \quad \epsilon_P : (\mathbf{F} \mathbf{S} \mathbf{F}^T) + \mathbf{L}_L = 0. \quad (2.30 \text{ a-c})$$

$$\rho_0 \frac{DU_L}{Dt} + \text{div } \mathbf{q}_L = -\mathbf{P}^T : \mathbf{Grad}(\mathbf{F} \mathbf{V}) + w_L. \quad (2.31)$$

Equations (2.30 a-c) are balance equations of the mass, linear and angular momentum and (2.31) is the balance equation of the internal energy, expressed on the undeformed configuration  $\Omega_0^{\text{Mec}}$ . The quantity  $\rho_0$  is the mass density (kg/m<sup>3</sup>),  $\mathbf{S}$  is the second Piola–Kirchhoff stress (N/m<sup>2</sup>) with  $\mathbf{S} = \mathbf{F}^{-1} \mathbf{P}$  where  $\mathbf{P}$  is the first Piola–Kirchhoff stress or nominal stress tensor with  $\mathbf{P} = J \boldsymbol{\sigma} \mathbf{F}^{-T}$ . The quantity  $\mathbf{f}_L$  is the volume force (N/m<sup>3</sup>),  $\mathbf{L}_L$  is the torque,  $U_L$  is the density of internal energy,  $\mathbf{q}_L$  is the heat flux density and  $w_L$  is the source term for the heat equation. The electromagnetic force which is a three differential form is transformed as:

$$\begin{aligned} \mathbf{f}_L &= J \mathbf{f}_E = \rho_L \mathbf{F}^{-T} \boldsymbol{\mathcal{E}} + J^{-1} ((\mathbf{F} \boldsymbol{\mathcal{J}}) \times (\mathbf{F} \boldsymbol{\mathcal{B}})) \\ &\quad + J \left( \mathbf{F}^{-T} \mathbf{Grad}(\mathbf{F}^{-T} \boldsymbol{\mathcal{E}}) \right)^T (J^{-1} \mathbf{F} \boldsymbol{\mathcal{P}}) \\ &\quad + \left( \mathbf{F}^{-T} \mathbf{Grad}(J^{-1} \mathbf{F} \boldsymbol{\mathcal{B}}) \right)^T (\mathbf{F}^{-T} \boldsymbol{\mathcal{M}}) \\ &\quad + J \frac{\partial}{\partial t} [J^{-2} (\mathbf{F} \boldsymbol{\mathcal{P}}) \times (\mathbf{F} \boldsymbol{\mathcal{B}})] + \text{Div} [J^{-1} \mathbf{V} \otimes [(\mathbf{F} \boldsymbol{\mathcal{P}}) \times (\mathbf{F} \boldsymbol{\mathcal{B}})]]. \end{aligned} \quad (2.32)$$

The torque and the internal energy are transformed as:

$$\mathbf{L}_L = J \mathbf{L}_E = (\mathbf{F} \boldsymbol{\mathcal{P}}) \times (\mathbf{F}^{-T} \boldsymbol{\mathcal{E}}) + (\mathbf{F}^{-T} \boldsymbol{\mathcal{M}}_{\text{eff}}) \times (\mathbf{F} \boldsymbol{\mathcal{B}}), \quad (2.33a)$$

$$\rho_0 \frac{DU_L}{Dt} = \rho_0 c_p \frac{\partial \vartheta_L}{\partial t}, \quad (2.33b)$$

where  $\vartheta_L$  is the temperature expressed on the undeformed configuration and the source term is obtained using the transformation:

$$w_L = J w_E = (\mathbf{F}\mathcal{J}) \cdot (\mathbf{F}^{-T}\mathcal{E}_{\text{eff}}) \quad (2.34a)$$

$$- J \left( \mathbf{F}^{-T} \mathcal{M}_{\text{eff}} \right) \times \left( \partial_t (J^{-1} \mathbf{F}\mathcal{B}) + \mathbf{Grad} (J^{-1} \mathbf{F}\mathcal{B}) \mathbf{V} \right) \quad (2.34b)$$

$$- \rho_0 \left( \frac{\partial}{\partial t} \left( \frac{\mathbf{F}\mathcal{P}}{\rho_0} \right) + \mathbf{Grad} \left( \frac{\mathbf{F}\mathcal{P}}{\rho_0} \right) \mathbf{V} \right) \cdot (\mathbf{F}^{-T} \mathcal{E}_{\text{eff}}). \quad (2.34c)$$

149

Equations (2.30)–(2.31) must be completed by constitutive laws which relate the stress tensor to its associated conjugate strain tensor. In this paper, we use the second Piola–Kirchhoff stress and the Green–Lagrange strain tensors. We assume the following nonlinear constitutive laws for the thermal and thermo-mechanical problems [37]:

$$\begin{aligned} \mathbf{q}_L &= J \mathbf{F}^{-1} \mathbf{Q}(\mathbf{Grad}(\vartheta_E \circ \varphi_t^{-1})) \\ &= \underbrace{J \mathbf{F}^{-1} \kappa_E \mathbf{F}^{-T}}_{\kappa_L} \mathbf{Grad} \vartheta_L = -\kappa_L(\vartheta_L) \mathbf{Grad} \vartheta_L, \end{aligned} \quad (2.35)$$

$$\mathbf{S} = \mathcal{S}_{\text{VEP}}(\mathbf{E}, \dot{\mathbf{E}}, \vartheta_L, \mathbf{Z}_L(\tau \leq t)), \quad \mathbf{E} = \frac{1}{2}(\mathbf{F}^T \mathbf{F} - \mathbf{1}), \quad (2.36 \text{ a-b})$$

150 where  $\kappa_L$  is the thermal conductivity tensor (W/mK) and  $\mathcal{S}_{\text{VEP}}$  is a mapping  
 151 that represents the visco-elastoplastic constitutive law. Viscosity is reflected  
 152 through the dependence of the stress on the rate of the Green–Lagrange ten-  
 153 sor  $\dot{\mathbf{E}}$ , plasticity is accounted for using a set of internal variables  $\mathbf{Z}_L(\tau \leq t)$   
 154 and the thermo-mechanical aspect is accounted for by the dependency on the  
 155 temperature  $\vartheta_L$ .

### 156 3. Formulations, discretization and linearization

157 In this section, we derive the simplified multiphysics problem from the fully  
 158 coupled problem defined in section 2. Using this simplified problem, strong  
 159 and weak formulations of the multiphysics problems are derived using poten-  
 160 tials. The weak formulations are then discretized in space using the continuous

161 Galerkin approximation and in time using the backward Euler integrator. Fi-  
 162 nally, the resulting nonlinear system of algebraic equations is linearized.

### 163 3.1. Simplified governing equations of the multiphysics problem

164 We make the following *magnetoquasistatic (MQS) assumptions*

$$\delta_i \simeq L_{\text{sys},i}, \quad \lambda \gg L_{\text{sys},i}. \quad (3.1)$$

165 In (3.1),  $\delta_i := 1/\sqrt{\pi f \sigma_{E,i} \mu_{E,i}}$  is the skin depth in the spatial direction  $i = x, y$   
 166 and  $z$ ,  $f$  is the frequency of the source term,  $\sigma_{E,i}$  and  $\mu_{E,i}$  are eigenvalues of  $\boldsymbol{\sigma}_E$   
 167 and  $\boldsymbol{\mu}_E$ ,  $\lambda$  is the wavelength corresponding to the frequency  $f$  and  $L_{\text{sys},i}$  is the  
 168 characteristic length of the structure in a spatial direction  $i$  [38]. The first term  
 169 of (3.1) explains the presence of eddy currents while the second explains the  
 170 neglect of electromagnetic waves. Further in this section, we will relax the first  
 171 condition in (3.1) to  $\delta_i = \alpha L_{\text{sys},i}$  with  $\alpha$  which is big thus allowing to neglect  
 172 the reaction field.

#### 173 3.1.1. The magnetoquasistatic problem

Using the MQS assumption, the following MQS problem in the deformed configuration can be defined:

$$\text{curl } \mathbf{h} = \mathbf{j}, \quad \text{curl } \mathbf{e} = -\partial_t \mathbf{b}, \quad \text{div } \mathbf{b} = 0, \quad (3.2 \text{ a-c})$$

together with the constitutive laws:

$$\mathbf{h} = \nu_E(\mathbf{b}) \mathbf{b} = \mathbf{H}(\mathbf{b}), \quad \mathbf{j} = \mathbf{j}_{\text{eff}} = \boldsymbol{\sigma}_E \mathbf{e}_{\text{eff}} + \mathbf{j}_s = \boldsymbol{\sigma}_E(\mathbf{e} + \mathbf{v} \times \mathbf{b}) + \mathbf{j}_s. \quad (3.3 \text{ a-b})$$

174

In Lagrangian setting, the MQS problem is governed by Maxwell's equations [20, 35]:

$$\text{Curl } \mathcal{H}_{\text{eff}} = \mathcal{J}, \quad \text{Curl } \mathcal{E}_{\text{eff}} = -\partial_t \mathcal{B}, \quad \text{Div } \mathcal{B} = 0 \quad (3.4 \text{ a-c})$$

completed by the following constitutive laws:

$$\mathcal{H}_{\text{eff}} = \nu_L \mathcal{B}, \quad \mathcal{J} = \sigma_L \mathcal{E}_{\text{eff}} + \mathcal{J}_s. \quad (3.5 \text{ a-b})$$

175

In addition to the MQS assumption, we assume *quasistatic mechanical problem* thus neglecting the inertia term in the balance of linear momentum and *isotropic magnetic materials* therefore restoring the symmetry of the Cauchy and the second Piola–Kirchhoff stress as  $\mathbf{L}_E = \mathbf{L}_L = \mathbf{0}$  in (2.22 c) and (2.30 c). Additionally, we neglect mechanical losses in the heat equation. Under these assumptions, balance equations in the deformed configuration become:

$$\frac{D\rho}{Dt} + \rho \operatorname{div} \mathbf{v} = 0, \quad \operatorname{div} \boldsymbol{\sigma} + \mathbf{f}_E = 0, \quad \boldsymbol{\sigma} = \boldsymbol{\sigma}^T. \quad (3.6 \text{ a-c})$$

$$\rho c_p \frac{\partial \vartheta_E}{\partial t} + \operatorname{div} \mathbf{q}_E = w_E \quad (3.7)$$

and the electromagnetic force, torque and electromagnetic losses in (2.24)–(2.27) become:

$$\mathbf{f}_E = \mathbf{j} \times \mathbf{b} + (\operatorname{grad} \mathbf{b})^T \mathbf{m}, \quad \mathbf{L}_E = \mathbf{m} \times \mathbf{b}, \quad w_E = \mathbf{j}_{\text{eff}} \cdot \mathbf{e}_{\text{eff}} - \mathbf{m}_{\text{eff}} \cdot \frac{\partial \mathbf{b}}{\partial t}. \quad (3.8 \text{ a-c})$$

In Lagrangian setting, the conservation equations become:

$$\rho_0 - \rho J = 0, \quad \operatorname{Div} \mathbf{F} \mathbf{S} + \mathbf{f}_L = \mathbf{0}, \quad \mathbf{S} = \mathbf{S}^T, \quad (3.9 \text{ a-c})$$

$$\rho_0 c_p \frac{\partial \vartheta_L}{\partial t} + \operatorname{Div} \mathbf{q}_L = w_L. \quad (3.10)$$

where the electromagnetic force and torque are given by:

$$\mathbf{f}_L = J^{-1} ((\mathbf{F} \mathcal{J}) \times (\mathbf{F} \mathcal{B})) + J \left( \mathbf{F}^{-T} \operatorname{Grad} (J^{-1} \mathbf{F} \mathcal{B}) \right)^T (\mathbf{F}^{-T} \mathcal{M}), \quad (3.11)$$

$$\mathbf{L}_L = \left( \mathbf{F}^{-T} \mathcal{M}_{\text{eff}} \right) \times (\mathbf{F} \mathcal{B}), \quad (3.12)$$

and the source term is given by:

$$w_L = (\mathbf{F} \mathcal{J}) \cdot (\mathbf{F}^{-T} \mathcal{E}_{\text{eff}}) - J(\mathbf{F}^{-T} \mathcal{M}_{\text{eff}}) \times [\partial_t (J^{-1} \mathbf{F} \mathcal{B}) + \operatorname{Grad} (J^{-1} \mathbf{F} \mathcal{B}) \mathbf{V}]. \quad (3.13)$$

Further in the paper, we consider elasto-plastic materials governed by the following constitutive law:

$$\mathbf{S} = \mathcal{S}_{EP}(\mathbf{E}, \vartheta_L, \mathbf{Z}_L(\tau \leq t)), \quad \mathbf{E} = \frac{1}{2}(\mathbf{F}^T \mathbf{F} - \mathbb{1}). \quad (3.14 \text{ a-b})$$

178 In this case, the second Piola–Kirchhoff stress does not depend on the rate of  
179 Green–Lagrange strain as viscosity is not considered.

### 180 3.2. Strong forms

#### 181 3.2.1. The magnetoquasistatic problem

The strong formulation of the MQS problem is derived using the so-called *magnetic induction conforming formulations* [39]. In the deformed configuration, the derivation is achieved by verifying equations (3.2 b-c) in the strong sense:

$$\mathbf{b} = \mathbf{curl} \mathbf{a} \simeq \mathbf{b}_s = \mathbf{curl} \mathbf{a}_s, \quad \mathbf{e} = -\partial_t \mathbf{a} - \mathbf{grad} \phi \simeq -\partial_t \mathbf{a}_s - \mathbf{grad} \phi \quad (3.15)$$

182 where  $\mathbf{a}$  is the vector potential unknown field used for the eddy currents problem,  
183  $\mathbf{a}_s$  is the source vector potential which can be pre-computed based on the electric  
184 current source  $\mathbf{j}_s$  imposed in inductors such as in coils and  $\phi$  is the unknown  
185 scalar potential. The approximation  $\mathbf{a} \simeq \mathbf{a}_s$  implies the neglect of the reaction  
186 field and is valid under the assumption  $\delta_i = \alpha L_{\text{sys},i}$  with  $\alpha$  which is big [40].

The electric potential  $\phi$  is governed by the following problem where (3.16) is obtained by applying the divergence  $\text{div}$  operator to (3.2 a) and (3.18) is derived from (3.3 b):

$$\text{div} \mathbf{j} = 0 \quad \text{in } \Omega_t^{\text{Ele}}, \quad (3.16)$$

$$\mathbf{j} = \boldsymbol{\sigma}_E(\mathbf{e} + \mathbf{v} \times \mathbf{b}) + \mathbf{j}_s \quad (3.17)$$

$$= \boldsymbol{\sigma}_E(-\partial_t \mathbf{a}_s - \mathbf{grad} \phi + \mathbf{v} \times \mathbf{curl} \mathbf{a}_s) + \mathbf{j}_s \quad \text{in } \Omega_t^{\text{Ele}}, \quad (3.18)$$

$$\phi(\mathbf{x}, t) = \phi_D(\mathbf{x}, t) \quad \text{on } \Gamma_t^{\text{Diri}, \text{Ele}}, \quad (3.19)$$

$$\mathbf{n}_E \cdot \mathbf{j} = 0 \quad \text{on } \Gamma_t^{\text{Neu}, \text{Ele}}. \quad (3.20)$$

187 (3.19) and (3.20) are the Dirichlet and the Neumann boundary conditions.

In the undeformed configuration, the derivation is carried out by verifying equations (3.4 b-c) in the strong sense:

$$\mathcal{B} = \text{Curl } \mathcal{A} \simeq \mathcal{B}_s = \text{Curl } \mathcal{A}_s = \text{Curl } (\mathbf{F}^T \mathbf{a}_s),$$

$$\mathcal{E}_{\text{eff}} = -\partial_t \mathcal{A} - \mathbf{Grad } \Phi \simeq -\partial_t \mathcal{A}_s - \mathbf{Grad } \Phi = -\mathbf{F}^T \partial_t \mathbf{a}_s - \mathbf{Grad } \Phi. \quad (3.21)$$

In (3.21), the 1 differential form  $\mathcal{A}_s$  is transformed as  $\mathcal{A}_s = \mathbf{F}^T \mathbf{a}_s$ . The electric potential  $\Phi$  is therefore governed by the following problem where (3.22) is obtained by applying the divergence operator  $\text{Div}$  to (3.4 a) and (3.24) is derived from (3.5 b):

$$\text{Div } \mathcal{J} = 0, \quad \text{in } \Omega_0^{\text{Ele}}, \quad (3.22)$$

$$\mathcal{J} = \sigma_L \mathcal{E}_{\text{eff}} + \mathcal{J}_s \quad (3.23)$$

$$= -\sigma_L (\mathbf{F}^T \partial_t \mathbf{a}_s + \mathbf{Grad } \Phi) + \mathcal{J}_s, \quad \text{in } \Omega_0^{\text{Ele}} \quad (3.24)$$

$$\Phi(\mathbf{x}, t) = \Phi_D(\mathbf{x}, t) \quad \text{on } \Gamma_0^{\text{Diri, Ele}}, \quad (3.25)$$

$$\mathbf{n}_L \cdot \mathcal{J} = 0 \quad \text{on } \Gamma_0^{\text{Neu, Ele}}. \quad (3.26)$$

188 where the conductivity tensor is transformed as  $\sigma_L = J \mathbf{F}^{-1} \sigma_E (\vartheta_E \circ \varphi_t^{-1}) \mathbf{F}^{-T}$   
 189 thanks to (2.21).

### 190 3.2.2. The heat equation

In the deformed configuration, the evolution of the temperature is governed by the following problem derived from (3.7) and (3.8 c) and (2.35):

$$\rho c_p \frac{\partial \vartheta_E}{\partial t} + \text{div } \mathbf{q}_E = w_E \quad \text{in } \Omega_t^{\text{The}}, \quad (3.27)$$

$$\mathbf{q}_E = -\kappa_E (\vartheta_E) \mathbf{grad } \vartheta_E \quad \text{in } \Omega_t^{\text{The}}, \quad (3.28)$$

$$\vartheta_E(\mathbf{x}, 0) = \vartheta_{E,0}(\mathbf{x}) \quad \text{in } \Omega_0^{\text{The}}, \quad (3.29)$$

$$\vartheta_E(\mathbf{x}, t) = \vartheta_{E,D}(\mathbf{x}, t) \quad \text{on } \Gamma_t^{\text{Diri, The}}, \quad (3.30)$$

$$\mathbf{n}_E \cdot \mathbf{q}_E = h_E(t) (\vartheta_E - \vartheta_{E,B}) \quad \text{on } \Gamma_t^{\text{conv, The}}, \quad (3.31)$$

$$\mathbf{n}_E \cdot \mathbf{q}_E = \epsilon_E^R \sigma_E^R (\vartheta_E^4 - \vartheta_{E,R}^4) \quad \text{on } \Gamma_t^{\text{rad, The}}. \quad (3.32)$$



The source term in (3.27) can be expressed in terms of the potentials as:

$$w_E = \underbrace{(\boldsymbol{\sigma}_E (\partial_t \mathbf{a}_s + \mathbf{grad} \phi - \mathbf{v} \times \mathbf{curl} \mathbf{a}_s))}_{w_E^{\text{eddy}}}{}^2 - \underbrace{\mathbf{j}_s \cdot (\boldsymbol{\sigma}_E (\partial_t \mathbf{a}_s + \mathbf{grad} \phi - \mathbf{v} \times \mathbf{curl} \mathbf{a}_s))}_{w_E^{\text{eddy}}} - \underbrace{\mathbf{m}_{\text{eff}} \cdot \mathbf{curl} \left( \frac{\partial \mathbf{a}_s}{\partial t} \right)}_{w_E^{\text{hyst}}} \quad (3.33)$$

191 where  $w_E^{\text{eddy}}$  and  $w_E^{\text{hyst}}$  represent eddy current and hysteretic losses. Equations  
 192 (3.29), (3.30), (3.31) and (3.32) represent the initial condition, Dirichlet, con-  
 193 vective and radiative boundary conditions, respectively.

The Lagrangian strong form of the heat problem is given by:

$$\rho_0 c_p \frac{\partial \vartheta_L}{\partial t} + \text{Div} \mathbf{q}_L = w_L \quad \text{in } \Omega_0^{\text{The}}, \quad (3.34)$$

$$\mathbf{q}_L = -\boldsymbol{\kappa}_L(\vartheta_L) \mathbf{Grad} \vartheta_L \quad \text{in } \Omega_0^{\text{The}}, \quad (3.35)$$

$$\vartheta_L(\mathbf{x}, 0) = \vartheta_{L,0}(\mathbf{x}) \quad \text{in } \Omega_0^{\text{The}}, \quad (3.36)$$

$$\vartheta_L(\mathbf{x}, t) = \vartheta_{L,D}(\mathbf{x}, t) \quad \text{on } \Gamma_0^{\text{Diri,The}}, \quad (3.37)$$

$$\mathbf{n}_L \cdot \mathbf{q}_L = h_L(t)(\vartheta_L - \vartheta_{L,B}) \quad \text{on } \Gamma_0^{\text{conv,The}}, \quad (3.38)$$

$$\mathbf{n}_L \cdot \mathbf{q}_L = \epsilon_L^R \sigma_L^R (\vartheta_L^4 - \vartheta_{L,R}^4) \quad \text{on } \Gamma_t^{\text{rad,The}} \quad (3.39)$$

194 where the thermal conductivity is transformed according to (2.21) as  $\boldsymbol{\kappa}_L =$   
 195  $J \mathbf{F}^{-1} \boldsymbol{\kappa}_E \mathbf{F}^{-T}$  and the convective heat coefficient  $h_L(t)$  is transformed using  
 196 Nanson's formula as  $h_L(t) = J |\mathbf{F}^{-T} \mathbf{n}_L| h_E(t)$ .

The source term in (3.34) can be expressed in terms of the potentials as:

$$w_L = (\underbrace{\mathbf{F}(\boldsymbol{\sigma}_L (\partial_t \mathcal{A}_s + \mathbf{Grad} \Phi) - \mathcal{J}_s)}_{-\mathcal{J}}) \cdot (\underbrace{\mathbf{F}^{-T} (\partial_t \mathcal{A}_s + \mathbf{Grad} \Phi)}_{-\mathcal{E}_{\text{eff}}}) +$$

$$J \mathbf{F}^{-T} \underbrace{\mu_0^{-1} (\mathbb{1} - \nu_L) \mathbf{Curl} \mathcal{A}_s}_{\mathcal{M}_{\text{eff}}} \left[ \partial_t (J^{-1} \mathbf{F} \mathbf{Curl} \mathcal{A}_s) + \mathbf{Grad} (J^{-1} \mathbf{F} \mathbf{Curl} \mathcal{A}_s) \right]. \quad (3.40)$$

197 Equations (3.36), (3.37), (3.38) and (3.39) represent the initial condition, Dirich-  
 198 let, convective and radiative boundary conditions, respectively.

199 *3.2.3. The mechanical problem*

Mechanical fields in the undeformed configuration are governed by the following problem:

$$\text{Div}(\mathbf{F}\mathbf{S}) + \mathbf{f}_L = 0 \quad \text{in } \Omega_0^{\text{Mec}}, \quad (3.41)$$

$$\mathbf{S} = \mathcal{S}_{EP}(\mathbf{E}, \vartheta_L, \mathbf{Z}_L(\tau \leq t)) \quad \text{in } \Omega_0^{\text{Mec}}, \quad (3.42)$$

$$\mathbf{E} = \frac{\mathbf{F}^T \mathbf{F} - \mathbb{1}}{2} \quad \text{in } \Omega_0^{\text{Mec}}, \quad (3.43)$$

$$\mathbf{u}(\mathbf{x}, t) = \mathbf{u}_D(\mathbf{x}, t) \quad \text{on } \Gamma_{0,D}^{\text{Mec}}. \quad (3.44)$$

$$\mathbf{n}_L \cdot (\mathbf{F}\mathbf{S}) = \mathbf{t}_L \quad \text{on } \Gamma_{0,N}^{\text{Mec}}. \quad (3.45)$$

In terms of the potential, the force  $\mathbf{f}_L$  in (3.11) is given by:

$$\begin{aligned} \mathbf{f}_L = \mathbf{F}_L(\mathbf{u}, \Phi) = J^{-1} \mathbf{F} & \underbrace{(\sigma_L(\partial_t \mathcal{A}_s + \mathbf{Grad} \Phi) + \mathcal{J}_s)}_{\mathcal{J}} \times \mathbf{F} \underbrace{\mathbf{Curl}(\mathcal{A}_s)}_{\mathcal{B}} + \\ J(\mathbf{F}^{-T} \mathbf{Grad}(J^{-1} \mathbf{F} \underbrace{\mathbf{Curl}(\mathcal{A}_s)}_{\mathcal{B})))^T} & \underbrace{(\mathbf{F}^{-T} \mu_0^{-1} \chi_{BL} J^{-1} \mathbf{F}^T \mathbf{F} \mathbf{Curl} \mathcal{A}_s)}_{\mathcal{M}}. \end{aligned} \quad (3.46)$$

The term  $\mathbf{t}_L$  in (3.45) represents the surface traction applied on part of the boundary  $\Gamma_{0,N}^{\text{Mec}}$ . The thermo-mechanical constitutive law (3.42)–(3.43) is derived from (3.14 a). In this paper, we use the constitutive law described in [30]. As a reminder, the total deformation gradient  $\mathbf{F}$  and the total deformation gradients in the glassy and rubbery states were given by:

$$\mathbf{F} = \mathbf{F}^{tg} = \mathbf{F}^{tr} = \mathbb{1} + \mathbf{Grad} \mathbf{u}, \quad (3.47)$$

where the superscript  $t$  denotes the total deformation gradient and the superscripts  $r$  and  $g$  were used for the rubbery and the glassy states. The total deformation gradients of both phases are decomposed as:

$$\mathbf{F}^{tg} = \mathbf{F}^g \mathbf{F}^f = \mathbf{F}^{eg} \mathbf{F}^{pg} \mathbf{F}^f, \mathbf{F}^{tr} = \mathbf{F}^r \mathbf{F}^p = \mathbf{F}^{er} \mathbf{F}^p, \quad (3.48)$$

200 where  $\mathbf{F}^{eg}$  and  $\mathbf{F}^{pg}$  are the deformation gradients for the elastic and plastic  
 201 phases in the glassy state,  $\mathbf{F}^f$  is the frozen deformation gradient that represents  
 202 the temporary deformation which is stored during high temperature shape fixing

203 and  $\mathbf{F}^r$  and  $\mathbf{F}^p$  are the elastic and plastic deformation gradients for the rubbery  
 204 state.

The total Cauchy stress was also given by:

$$\boldsymbol{\sigma} = z^g \boldsymbol{\sigma}^g + (1 - z^g) \boldsymbol{\sigma}^r, \quad (3.49)$$

where the temperature-dependent parameter  $z^g$  is the ratio of the glassy state. Using the second Piola–Kirchhoff stress and Green–Lagrange strain tensors, the following expression of the stress tensor can be derived:

$$\begin{aligned} \mathbf{S} &= J \mathbf{F}^{-1} \boldsymbol{\sigma} \mathbf{F}^{-T} = z^g J \mathbf{F}^{-1} \boldsymbol{\sigma}^g \mathbf{F}^{-T} + (1 - z^g) J \mathbf{F}^{-1} \boldsymbol{\sigma}^r \mathbf{F}^{-T} \\ &= z^g J^f \mathbf{F}^{f-1} \underbrace{\left( J^g \mathbf{F}^{g-1} \boldsymbol{\sigma}^g \mathbf{F}^{g-T} \right)}_{\mathbf{S}^g} \mathbf{F}^{f-T} \\ &\quad + (1 - z^g) J^p \mathbf{F}^{p-1} \underbrace{\left( J^r \mathbf{F}^{r-1} \boldsymbol{\sigma}^r \mathbf{F}^{r-T} \right)}_{\mathbf{S}^r} \mathbf{F}^{p-T}. \end{aligned} \quad (3.50)$$

In (3.50),  $\mathbf{S}^g$  and  $\mathbf{S}^r$  are the second Piola–Kirchhoff stress tensors defined on the intermediate configurations [30] by:

$$\mathbf{S}^g = (\mathbf{F}^{pg})^{-1} (\lambda^g \text{tr}(\mathbf{E}^{eg}) \mathbf{1} + 2\mu^g \mathbf{E}^{eg}) (\mathbf{F}^{pg})^{-T}, \quad (3.51)$$

$$\mathbf{S}^r = \lambda^r \text{tr}(\mathbf{E}^{er}) \mathbf{1} + 2\mu^r \mathbf{E}^{er}. \quad (3.52)$$

205 The parameters  $\lambda^g$ ,  $\lambda^r$ ,  $\mu^g$  and  $\mu^r$  are Lamé parameters for the glassy and the  
 206 rubbery states. Determinants of deformation gradients of intermediate configurations are defined as  $J^i = \det \mathbf{F}^i$  where the superscript  $i$  refer to configurations  
 207 of the glassy state ( $^g$ ,  $^{eg}$  and  $^{pg}$ ) or of the rubbery state ( $^{er}$  and  $^p$ ). The contribu-  
 208 tion to the stress due to thermal expansion have been neglected in (3.51)–(3.52).  
 209

210 Details on the equations that govern the evolution of internal variables  
 211  $\mathbf{Z}_L(\tau \leq t) := (z^g, \mathbf{F}^f, \mathbf{F}^p, \mathbf{F}^{pg})$  and the numerical update of the internal vari-  
 212 ables can be found in [30].

### 213 3.3. Weak forms

The weak forms of the electromagnetic problem (3.22)–(3.26), the heat problem (3.34)–(3.39) and the mechanical problem (3.41)–(3.45) read [39, 41, 31, 42]:

for each  $t \in \mathcal{I}_t$ , find  $(\Phi \times \vartheta_L \times \mathbf{u}) \in U \times V \times \mathbf{W}$  such that

$$\int_{\Omega_0^{\text{Ele}}} \boldsymbol{\sigma}_L \mathbf{Grad} \Phi \cdot \mathbf{Grad} \Phi' \, d\Omega_0 + \int_{\Omega_0^{\text{Ele}}} \boldsymbol{\sigma}_L \partial_t \mathcal{A}_s \cdot \mathbf{Grad} \Phi' \, d\Omega_0 = 0, \quad (3.53)$$

$$\begin{aligned} & \int_{\Omega_0^{\text{The}}} \rho_0 c_p \frac{\partial \vartheta_L}{\partial t} \cdot \vartheta_L' \, d\Omega_0 + \int_{\Omega_0^{\text{The}}} \underbrace{\boldsymbol{\kappa}_L \mathbf{Grad} \vartheta_L}_{-\mathbf{q}_L} \cdot \mathbf{Grad} \vartheta_L' \, d\Omega_0 - \\ & \int_{\Omega_0^{\text{The}}} \underbrace{(\mathbf{F}(\boldsymbol{\sigma}_L(\partial_t \mathcal{A}_s + \mathbf{Grad} \Phi) - \mathcal{J}_s)) \cdot (\mathbf{F}^{-T}(\partial_t \mathcal{A}_s + \mathbf{Grad} \Phi))}_{w_L} \cdot \vartheta_L' \, d\Omega_0 \\ & + \int_{\Gamma_0^{\text{conv, The}}} \underbrace{h_L(t)(\vartheta_L - \vartheta_{L,B})}_{\mathbf{n}_L \cdot \mathbf{q}_L} \cdot \vartheta_L' \, d\Gamma_0 + \\ & \int_{\Gamma_0^{\text{rad, The}}} \underbrace{\epsilon_L^R \sigma_L^R (\vartheta_L^4 - \vartheta_{L,R}^4)}_{\mathbf{n}_L \cdot \mathbf{q}_L} \cdot \vartheta_L' \, d\Gamma_0 = 0 \quad (3.54) \end{aligned}$$

$$\begin{aligned} & \int_{\Omega_0^{\text{Mec}}} \mathcal{S}_{EP}(\mathbf{u}, \vartheta_L, \mathbf{Z}_L) : \delta \mathbf{E} \, d\Omega_0 - \\ & \int_{\Omega_0^{\text{Mec}}} \mathbf{F}_L(\mathbf{u}, \Phi) \cdot \mathbf{u}' \, d\Omega_0 = \int_{\Gamma_0^{\text{N}}} \mathbf{t}_L \cdot \mathbf{u}' \, d\Gamma_0 \quad (3.55) \end{aligned}$$

214 holds for all test functions  $(\Phi' \times \vartheta_L' \times \mathbf{u}') \in (U_0 \times V_0 \times \mathbf{W}_0)$ . The force  $\mathbf{f}_L =$   
 215  $\mathbf{F}_L(\mathbf{u}, \Phi)$  is given by (3.46) and the dependence on the displacement is achieved  
 216 through  $J$  and  $\mathbf{F}$ . The function spaces are defined such that  $U \subseteq H^1(\Omega_0^{\text{Ele}})$ ,  
 217  $V \subseteq H^1(\Omega_0^{\text{The}})$ ,  $\mathbf{W} \subseteq \mathbf{H}^1(\Omega^{\text{Mec}}) \equiv (H^1(\Omega^{\text{Mec}}))^3$  and the source term of the  
 218 electromagnetic problem  $\mathcal{A}_s$  belongs to a subspace of  $\mathbf{H}(\mathbf{Curl}; \Omega_0^{\text{Ele}})$ . The vir-  
 219 tual Green–Lagrange strain  $\delta \mathbf{E}$  is related to the virtual displacement  $\mathbf{u}'$  through  
 220  $\delta \mathbf{E} = \mathbf{F}^T \mathbf{Grad} \mathbf{u}'$ .

### 221 3.4. Spatial and temporal discretization

The unknown fields  $\Phi$ ,  $\vartheta_L$  and  $\mathbf{u}$  in (3.53)–(3.55) belong to infinite dimensional functional spaces. For numerical simulation, these fields need to be approximated by finite dimensional spaces

$$\Phi(\mathbf{x}, t) \approx \bar{\Phi}(\mathbf{x}, t), \quad \vartheta_L(\mathbf{x}, t) \approx \bar{\vartheta}_L(\mathbf{x}, t), \quad \mathbf{u}(\mathbf{x}, t) \approx \bar{\mathbf{u}}(\mathbf{x}, t) \quad (3.56)$$

defined by:

$$\bar{\Phi}(\mathbf{x}, t) = \sum_{i=1}^{N^{\text{Ele}}} \bar{\Phi}_i(t) N_i^{\text{Ele}}(\mathbf{x}), \quad \mathbf{Grad} \bar{\Phi}(\mathbf{x}) = \sum_{i=1}^{N^{\text{Ele}}} \bar{\Phi}_i(t) \mathbf{Grad} N_i^{\text{Ele}}(\mathbf{x}), \quad (3.57)$$

$$\bar{\vartheta}_L(\mathbf{x}, t) = \sum_{i=1}^{N^{\text{The}}} \bar{\vartheta}_i(t) N_i^{\text{The}}(\mathbf{x}), \quad \mathbf{Grad} \bar{\vartheta}_L(\mathbf{x}) = \sum_{i=1}^{N^{\text{The}}} \bar{\vartheta}_i(t) \mathbf{Grad} N_i^{\text{The}}(\mathbf{x}), \quad (3.58)$$

$$\bar{\mathbf{u}}(\mathbf{x}, t) = \sum_{i=1}^{N^{\text{Mec}}} \bar{\mathbf{u}}_i(t) N_i^{\text{Mec}}(\mathbf{x}), \quad \mathbf{Grad} \bar{\mathbf{u}}(\mathbf{x}) = \sum_{i=1}^{N^{\text{Mec}}} \bar{\mathbf{u}}_i(t) \mathbf{Grad} N_i^{\text{Mec}}(\mathbf{x}), \quad (3.59)$$

222 where  $N^{\text{Ele}}$ ,  $N^{\text{The}}$  and  $N^{\text{Mec}}$  are the number of nodes of the electromagnetic,  
 223 thermal and mechanical domains,  $\bar{\Phi}_i$ ,  $\bar{\vartheta}_i$  and  $\bar{\mathbf{u}}_i = (\bar{u}_{i,x}, \bar{u}_{i,y}, \bar{u}_{i,z})$  are degrees of  
 224 freedom and  $N_i^{\text{Ele}}$ ,  $N_i^{\text{The}}$  and  $N_i^{\text{Mec}}$  are shape functions for the electromagnetic,  
 225 thermal and mechanical problems, respectively.

Inserting (3.57)–(3.59) into (3.53)–(3.55) leads to the following discrete system of equations:

$$\mathbf{K}^{\text{Ele}}(\bar{\vartheta}, \bar{\mathbf{u}}) \bar{\Phi} + \mathbf{F}^{\text{Ele}}(\bar{\vartheta}, \bar{\mathbf{u}}) = \mathbf{0}, \quad (3.60)$$

$$\mathbf{M}^{\text{The}} \frac{D\bar{\vartheta}}{Dt} + \mathbf{K}^{\text{The}}(\bar{\vartheta}, \bar{\mathbf{u}}) \bar{\vartheta} + \mathbf{F}^{\text{The}}(\bar{\Phi}, \bar{\vartheta}, \bar{\mathbf{u}}) = \mathbf{0}, \quad (3.61)$$

$$\mathbf{K}^{\text{Mec}}(\bar{\vartheta}, \bar{\mathbf{u}}, \mathbf{Z}_L) + \bar{\mathbf{F}}^{\text{Mec}}(\bar{\Phi}, \bar{\mathbf{u}}) = \mathbf{0}. \quad (3.62)$$

where  $\bar{\Phi}$ ,  $\bar{\vartheta}_L$  and  $\bar{\mathbf{u}}$  are vectors of degrees of freedom and the matrices in (3.60)–

(3.62) are given by:

$$\mathbf{K}^{\text{Ele}} = \sum_{e=1}^{N^{\text{Ele}}} \mathbf{L}^{eT} \left[ \int_{\Omega_e} (\mathbf{B}^e)^T \boldsymbol{\sigma}_L(\bar{\mathbf{u}}, \bar{\boldsymbol{\vartheta}}) \mathbf{B}^e d\Omega_e \right] \mathbf{L}^{eT}, \quad (3.63)$$

$$\mathbf{F}^{\text{Ele}} = \sum_{e=1}^{N^{\text{Ele}}} \mathbf{L}^{eT} \left[ \int_{\Omega_e} (\mathbf{B}^e)^T \boldsymbol{\sigma}_L(\bar{\mathbf{u}}, \bar{\boldsymbol{\vartheta}}) \mathcal{A}_s^e d\Omega_e \right], \quad (3.64)$$

$$\mathbf{M}^{\text{The}} = \sum_{e=1}^{N^{\text{The}}} \mathbf{L}^{eT} \left[ \int_{\Omega_e} (\mathbf{N}^e)^T \rho_0 c_p \mathbf{N}^e d\Omega_e \right] \mathbf{L}^{eT}, \quad (3.65)$$

$$\mathbf{K}^{\text{The}} = \sum_{e=1}^{N^{\text{The}}} \mathbf{L}^{eT} \left[ \int_{\Omega_e} (\mathbf{B}^e)^T \boldsymbol{\kappa}_L(\bar{\mathbf{u}}, \bar{\boldsymbol{\vartheta}}) \mathbf{B}^e d\Omega_e \right] \mathbf{L}^{eT}, \quad (3.66)$$

$$\mathbf{F}^{\text{The}} = \sum_{e=1}^{N^{\text{The}}} \mathbf{L}^{eT} \left[ \int_{\Omega_e} (\mathbf{B}^e)^T \bar{w}_L(\bar{\mathbf{u}}, \bar{\boldsymbol{\vartheta}}, \bar{\boldsymbol{\Phi}}) d\Omega_e \right], \quad (3.67)$$

$$\mathbf{K}^{\text{Mec}} = \sum_{e=1}^{N^{\text{Mec}}} \mathbf{L}^{eT} \left[ \int_{\Omega_e} (\mathbf{B}^e)^T \boldsymbol{\mathcal{S}}_{EP}(\bar{\mathbf{u}}, \bar{\boldsymbol{\vartheta}}, \mathbf{Z}_L) d\Omega_e \right], \quad (3.68)$$

$$\mathbf{F}^{\text{Mec}} = \sum_{e=1}^{N^{\text{Mec}}} \mathbf{L}^{eT} \left[ \int_{\Omega_e} (\mathbf{N}^e)^T \mathbf{F}_L(\bar{\mathbf{u}}, \bar{\boldsymbol{\Phi}}) d\Omega_e \right] \quad (3.69)$$

where  $\mathbf{L}^e$  is the gather matrix,  $\mathbf{N}^e$  is the element shape function matrix,  $\mathbf{B}^e$  is composed of the elements of the gradient of  $\mathbf{N}^e$  [43, 31] and where we neglected the boundary terms in (3.53)–(3.55). The recurrent dependence on the displacement field in (3.60)–(3.62) and (3.63)–(3.69) results from the transformations between the deformed and undeformed configurations which involve the deformation gradient  $\mathbf{F}$  and its determinant  $J$ , and the electric conductivity  $\boldsymbol{\sigma}_L(\bar{\mathbf{u}}, \bar{\boldsymbol{\vartheta}})$  is considered to be temperature-dependent.

Equations (3.60)–(3.62) can be written as a system of differential algebraic equations:

$$\underbrace{\begin{pmatrix} \mathbf{0} & \mathbf{0} & \mathbf{0} \\ \mathbf{0} & \mathbf{M}^{\text{The}} & \mathbf{0} \\ \mathbf{0} & \mathbf{0} & \mathbf{0} \end{pmatrix}}_{\mathbf{M}} \underbrace{\frac{D}{Dt} \begin{pmatrix} \bar{\boldsymbol{\Phi}} \\ \bar{\boldsymbol{\vartheta}} \\ \bar{\mathbf{u}} \end{pmatrix}}_{\bar{\mathbf{v}}} + \underbrace{\begin{pmatrix} \mathbf{K}^{\text{Ele}}(\bar{\boldsymbol{\vartheta}}, \bar{\mathbf{u}}) \bar{\boldsymbol{\Phi}} + \mathbf{F}^{\text{Ele}}(\bar{\boldsymbol{\vartheta}}, \bar{\mathbf{u}}) \\ \mathbf{K}^{\text{The}}(\bar{\boldsymbol{\vartheta}}, \bar{\mathbf{u}}) \bar{\boldsymbol{\vartheta}} + \mathbf{F}^{\text{The}}(\bar{\boldsymbol{\Phi}}, \bar{\boldsymbol{\vartheta}}, \bar{\mathbf{u}}) \\ \mathbf{K}^{\text{Mec}}(\bar{\boldsymbol{\vartheta}}, \bar{\mathbf{u}}, \mathbf{Z}_L) + \bar{\mathbf{F}}^{\text{Mec}}(\bar{\boldsymbol{\Phi}}, \bar{\mathbf{u}}) \end{pmatrix}}_{\mathbf{f}(\bar{\mathbf{v}}, \mathbf{Z}_L)} = \begin{pmatrix} \mathbf{0} \\ \mathbf{0} \\ \mathbf{0} \end{pmatrix} \quad (3.70)$$

or

$$\mathbf{M} \frac{D\bar{\mathbf{v}}}{Dt} + \mathbf{f}(\bar{\mathbf{v}}, \mathbf{Z}_L) = \mathbf{0}, \quad (3.71)$$

where  $\mathbf{M}$  is a singular matrix and

$$\begin{aligned} \mathbf{f}_1 &= \mathbf{K}^{\text{Ele}}(\bar{\boldsymbol{\vartheta}}, \bar{\mathbf{u}}) \bar{\boldsymbol{\Phi}} + \mathbf{F}^{\text{Ele}}(\bar{\boldsymbol{\vartheta}}, \bar{\mathbf{u}}), \mathbf{f}_2 = \mathbf{K}^{\text{The}}(\bar{\boldsymbol{\vartheta}}, \bar{\mathbf{u}}) \bar{\boldsymbol{\vartheta}} + \mathbf{F}^{\text{The}}(\bar{\boldsymbol{\Phi}}, \bar{\boldsymbol{\vartheta}}, \bar{\mathbf{u}}), \\ \mathbf{f}_3 &= \mathbf{K}^{\text{Mec}}(\bar{\boldsymbol{\vartheta}}, \bar{\mathbf{u}}, \mathbf{Z}_L) + \bar{\mathbf{F}}^{\text{Mec}}(\bar{\boldsymbol{\Phi}}, \bar{\mathbf{u}}). \end{aligned} \quad (3.72)$$

Equation (3.71) can be discretized in time using the backward Euler integrator:

$$\mathbf{M} \frac{\bar{\mathbf{v}}^{n+1} - \bar{\mathbf{v}}^n}{\Delta t} + \mathbf{f}(\bar{\mathbf{v}}^{n+1}, \mathbf{Z}_L) = \mathbf{0}, \quad (3.73)$$

where  $\bar{\mathbf{v}}^{n+1} = \bar{\mathbf{v}}(t_{n+1})$  with  $t_{n+1} = t_0 + (n+1)\Delta t$  and  $\Delta t$  which is the time step. After reordering the terms of (3.73), the following nonlinear equations can be derived:

$$\begin{aligned} \mathbf{M} \bar{\mathbf{v}}^{n+1} + \Delta t \mathbf{f}(\bar{\mathbf{v}}^{n+1}, \mathbf{Z}_L) - \mathbf{M} \bar{\mathbf{v}}^n &= \mathbf{G}(\bar{\mathbf{v}}^{n+1}, \mathbf{Z}_L) - \mathbf{M} \bar{\mathbf{v}}^n \\ &= \mathbf{H}(\bar{\boldsymbol{\Phi}}^{n+1}, \bar{\boldsymbol{\vartheta}}^{n+1}, \bar{\mathbf{u}}^{n+1}, \mathbf{Z}_L) - \mathbf{M} \bar{\mathbf{v}}^n = \mathbf{0} \end{aligned} \quad (3.74)$$

233 with the vector function  $\mathbf{H} = (\mathbf{H}_1, \mathbf{H}_2, \mathbf{H}_3)$  defined such that  $\mathbf{H}_i(\bar{\boldsymbol{\Phi}}^{n+1}, \bar{\boldsymbol{\vartheta}}^{n+1}, \bar{\mathbf{u}}^{n+1}, \mathbf{Z}_L) :=$   
 234  $\mathbf{G}_i(\bar{\mathbf{v}}^{n+1}, \mathbf{Z}_L)$  for  $i = 1, 2$  or  $3$ .

### 235 3.5. Linearization

Equation (3.74) can be solved using the Newton–Raphson method. To do this, an iterative schema is used with the following linearization:

$$\begin{aligned} \mathbf{G}(\bar{\mathbf{v}}^{n+1}, \mathbf{Z}_L) &\simeq \mathbf{G}(\bar{\mathbf{v}}_m^{n+1}, \mathbf{Z}_L) + \left( \frac{\partial \mathbf{G}}{\partial \bar{\mathbf{v}}^{n+1}} \right)_{\bar{\mathbf{v}}_m^{n+1}} (\bar{\mathbf{v}}_{m+1}^{n+1} - \bar{\mathbf{v}}_m^{n+1}) \\ &= \mathbf{b}_{\text{RHS}}(\bar{\mathbf{v}}_m^{n+1}) - \mathbf{A}(\bar{\mathbf{v}}_m^{n+1}) \Delta \bar{\mathbf{v}}_{m+1}^{n+1} = \mathbf{0}, \end{aligned} \quad (3.75)$$

where the index  $m$  is used to denote the Newton–Raphson iteration. The terms in (3.75) are given by:

$$\begin{aligned} \mathbf{b}_{\text{RHS}} &= \mathbf{G}(\bar{\mathbf{v}}_m^{n+1}, \mathbf{Z}_L) = \mathbf{H}(\bar{\boldsymbol{\Phi}}_m^{n+1}, \bar{\boldsymbol{\vartheta}}_m^{n+1}, \bar{\mathbf{u}}_m^{n+1}, \mathbf{Z}_L) \\ &= \begin{pmatrix} \mathbf{H}_1(\bar{\boldsymbol{\Phi}}_m^{n+1}, \bar{\boldsymbol{\vartheta}}_m^{n+1}, \bar{\mathbf{u}}_m^{n+1}) \\ \mathbf{H}_2(\bar{\boldsymbol{\Phi}}_m^{n+1}, \bar{\boldsymbol{\vartheta}}_m^{n+1}, \bar{\mathbf{u}}_m^{n+1}) \\ \mathbf{H}_3(\bar{\boldsymbol{\Phi}}_m^{n+1}, \bar{\boldsymbol{\vartheta}}_m^{n+1}, \bar{\mathbf{u}}_m^{n+1}, \mathbf{Z}_L) \end{pmatrix}. \end{aligned} \quad (3.76)$$

236 The term  $\mathbf{H}_3$  depends on the internal variables  $\mathbf{Z}_L(\tau \leq t)$  through the second  
 237 Piola–Kirchhoff stress  $\mathbf{S}$ . For each quadrature point, the stress is updated using  
 238 the return mapping described in [30].

The stiffness matrix is given by:

$$\left( \frac{\partial \mathbf{G}}{\partial \bar{\mathbf{v}}^{n+1}} \right)_{\bar{\mathbf{v}}_m^{n+1}} = \mathbf{A} = \begin{pmatrix} \frac{\partial \mathbf{H}_1}{\partial \bar{\Phi}^{n+1}} & \frac{\partial \mathbf{H}_1}{\partial \bar{\vartheta}^{n+1}} & \frac{\partial \mathbf{H}_1}{\partial \bar{\mathbf{u}}^{n+1}} \\ \frac{\partial \mathbf{H}_2}{\partial \bar{\Phi}^{n+1}} & \frac{\partial \mathbf{H}_2}{\partial \bar{\vartheta}^{n+1}} & \frac{\partial \mathbf{H}_2}{\partial \bar{\mathbf{u}}^{n+1}} \\ \frac{\partial \mathbf{H}_3}{\partial \bar{\Phi}^{n+1}} & \frac{\partial \mathbf{H}_3}{\partial \bar{\vartheta}^{n+1}} & \frac{\partial \mathbf{H}_3}{\partial \bar{\mathbf{u}}^{n+1}} \end{pmatrix}. \quad (3.77)$$

The terms of the tangent stiffness matrix in (3.77) are given by:

$$\left( \frac{\partial \mathbf{H}_1}{\partial \bar{\Phi}^{n+1}} \right)_{\bar{\mathbf{v}}_m^{n+1}} = \left( \mathbf{K}^{\text{Ele}} \right)_{\bar{\Phi}_m^{n+1}, \bar{\vartheta}_m^{n+1}, \bar{\mathbf{u}}_m^{n+1}}, \quad (3.78)$$

$$\left( \frac{\partial \mathbf{H}_1}{\partial \bar{\vartheta}^{n+1}} \right)_{\bar{\mathbf{v}}_m^{n+1}} = \left( \frac{\partial \mathbf{K}^{\text{Ele}}}{\partial \bar{\vartheta}^{n+1}} \bar{\Phi}_m^{n+1} + \frac{\partial \mathbf{F}^{\text{Ele}}}{\partial \bar{\vartheta}^{n+1}} \right)_{\bar{\Phi}_m^{n+1}, \bar{\vartheta}_m^{n+1}, \bar{\mathbf{u}}_m^{n+1}}, \quad (3.79)$$

$$\left( \frac{\partial \mathbf{H}_1}{\partial \bar{\mathbf{u}}^{n+1}} \right)_{\bar{\mathbf{v}}_m^{n+1}} = \left( \frac{\partial \mathbf{K}^{\text{Ele}}}{\partial \bar{\mathbf{u}}^{n+1}} \bar{\Phi}_m^{n+1} + \frac{\partial \mathbf{F}^{\text{Ele}}}{\partial \bar{\mathbf{u}}^{n+1}} \right)_{\bar{\Phi}_m^{n+1}, \bar{\vartheta}_m^{n+1}, \bar{\mathbf{u}}_m^{n+1}}, \quad (3.80)$$

$$\left( \frac{\partial \mathbf{H}_2}{\partial \bar{\Phi}^{n+1}} \right)_{\bar{\mathbf{v}}_m^{n+1}} = \Delta t \left( \frac{\partial \mathbf{F}^{\text{The}}}{\partial \bar{\Phi}^{n+1}} \right)_{\bar{\Phi}_m^{n+1}, \bar{\vartheta}_m^{n+1}, \bar{\mathbf{u}}_m^{n+1}}, \quad (3.81)$$

$$\left( \frac{\partial \mathbf{H}_2}{\partial \bar{\vartheta}^{n+1}} \right)_{\bar{\mathbf{v}}_m^{n+1}} = \left( \mathbf{M}^{\text{The}} + \Delta t \left( \mathbf{K}^{\text{The}} + \frac{\partial \mathbf{K}^{\text{The}}}{\partial \bar{\vartheta}^{n+1}} \bar{\vartheta}_m^{n+1} + \frac{\partial \mathbf{F}^{\text{The}}}{\partial \bar{\vartheta}^{n+1}} \right) \right)_{\bar{\Phi}_m^{n+1}, \bar{\vartheta}_m^{n+1}, \bar{\mathbf{u}}_m^{n+1}}, \quad (3.82)$$

$$\left( \frac{\partial \mathbf{H}_2}{\partial \bar{\mathbf{u}}^{n+1}} \right)_{\bar{\mathbf{v}}_m^{n+1}} = \Delta t \left( \frac{\partial \mathbf{K}^{\text{The}}}{\partial \bar{\mathbf{u}}^{n+1}} \bar{\vartheta}_m^{n+1} + \frac{\partial \mathbf{F}^{\text{The}}}{\partial \bar{\mathbf{u}}^{n+1}} \right)_{\bar{\Phi}_m^{n+1}, \bar{\vartheta}_m^{n+1}, \bar{\mathbf{u}}_m^{n+1}}, \quad (3.83)$$

$$\left( \frac{\partial \mathbf{H}_3}{\partial \bar{\Phi}^{n+1}} \right)_{\bar{\mathbf{v}}_m^{n+1}} = \left( \frac{\partial \mathbf{F}^{\text{Mec}}}{\partial \bar{\Phi}^{n+1}} \right)_{\bar{\Phi}_m^{n+1}, \bar{\mathbf{u}}_m^{n+1}}, \quad (3.84)$$

$$\left( \frac{\partial \mathbf{H}_3}{\partial \bar{\vartheta}^{n+1}} \right)_{\bar{\mathbf{v}}_m^{n+1}} = \left( \frac{\partial \mathbf{K}^{\text{Mec}}}{\partial \bar{\vartheta}^{n+1}} \right)_{\bar{\vartheta}_m^{n+1}, \bar{\mathbf{u}}_m^{n+1}}, \quad (3.85)$$

$$\left( \frac{\partial \mathbf{H}_3}{\partial \bar{\mathbf{u}}^{n+1}} \right)_{\bar{\mathbf{v}}_m^{n+1}} = \left( \frac{\partial \mathbf{K}^{\text{Mec}}}{\partial \bar{\mathbf{u}}^{n+1}} + \frac{\partial \mathbf{F}^{\text{Mec}}}{\partial \bar{\mathbf{u}}^{n+1}} \right)_{\bar{\Phi}_m^{n+1}, \bar{\vartheta}_m^{n+1}, \bar{\mathbf{u}}_m^{n+1}}. \quad (3.86)$$

In (3.86), the first term is given by

$$\left( \frac{\partial \mathbf{K}^{\text{Mec}}}{\partial \bar{\mathbf{u}}^{n+1}} \right)_{\bar{\mathbf{v}}_m^{n+1}} = \sum_{e=1}^{N^{\text{Mec}}} \mathbf{L}^{eT} \left[ \int_{\Omega_e} (\mathbf{B}^e)^T \left( \frac{\partial \mathbf{S}_{EP}}{\partial \mathbf{E}} : \frac{\partial \mathbf{E}}{\partial \bar{\mathbf{u}}^{n+1}} \right) d\Omega_e \right]. \quad (3.87)$$



239 The Jacobian of the mechanical problem  $\partial \mathcal{S}_{EP}/\partial \mathbf{E}$  in (3.86) is also updated  
 240 using the return mapping algorithm described in [30]. The pseudocode in Algo-  
 241 rithm 1 illustrates the flow of the numerical code used to solve the multiphysics  
 242 problem.

---

**Algorithm 1** Pseudocode of the multiphysics SMP problem

---

**INPUT:** Mesh, current source  $I_s(t)$  and constitutive laws.

**OUTPUT:** Mechanical, thermal and electromagnetic fields, and Joule losses

**procedure** MULTIPHYSICS PROBLEM

$t \leftarrow t_0$ , initialization of the physical fields  $T|_{t_0} = T_0$  and  $\mathbf{u}|_{t_0} = \mathbf{u}_0$ ,

**for** ( $n \leftarrow 1$  To  $N_{TS}$ ) **do** *▷ the time loop (index  $n$ )*

**for** ( $m \leftarrow 1$  To  $N_{NR}^M$ ) **do** *▷ the NR loop of the overall problem*

**for** ( $l \leftarrow 1$  To  $N_{RM}$ ) **do** *▷ the NR loop of the return mapping*

            Pass internal variables as input,

            Update the mechanical law  $\mathbf{S}$  and  $\partial \mathcal{S}_{EP}/\partial \mathbf{E}$  using the RM

**end for**

        Update and compute the Jacobian,

        Assemble  $(\partial \mathbf{G}/\partial \bar{\mathbf{v}}^{n+1})_{\bar{\mathbf{v}}_{m+1}^{n+1}}$  from (3.77) and  $\mathbf{G}(\bar{\mathbf{v}}_m^{n+1})$  from (3.76),

        Solve the system  $(\partial \mathbf{G}/\partial \bar{\mathbf{v}}^{n+1})_{\bar{\mathbf{v}}_{m+1}^{n+1}} \Delta \mathbf{v}_{m+1}^{n+1} = -\mathbf{G}(\bar{\mathbf{v}}_m^{n+1}, \mathbf{Z}_L)$ ,

        compute the residual  $\mathbf{r}(\mathbf{v}_m^{n+1}) = \mathbf{G}(\bar{\mathbf{v}}_m^{n+1})$ ,

**if** ( $\|\mathbf{r}(\mathbf{v}_m^{n+1})\| \leq \varepsilon_{tol}$ ) **then**

            Exit the nonlinear loop of the overall problem

**else**

            Do another NR iteration for the overall problem

**end if**

**end for**

    Go to the next time step  $t \leftarrow t + \Delta t$

**end for**

**end procedure**

---

#### 243 4. Numerical Tests

244 This section is devoted to the numerical testing of the electro-thermo-mechanical  
 245 problem. A set of numerical tests similar to the ones developed in [30] are herein  
 246 proposed. Whereas the authors in [30] considered ideal and non-ideal shape  
 247 memory polymer materials, the main focus of this paper is on the fully coupled  
 248 problem. Therefore, in Section 4.1 we consider an ideal and a non-ideal shape  
 249 memory polymer single element similar to the one in [30] for the validation of  
 250 the thermomechanical problem. In Section 4.2 we only consider an ideal shape  
 251 memory polymer stent for the fully coupled electro-thermo-mechanical problem.

252 The two considered tests are:

- 253 • the uniaxial tests on a  $1 \times 1 \times 1 \text{ mm}^3$  single-element cube (SEC),
- 254 • the simulation of a cylindrical vascular stent (CVS) similar to the one de-  
 255 scribed in [30]. The stent has the same dimensions and material properties  
 256 but without the small holes.

Symbol	Value	Unit
$E^r$	0.9	MPa
$E^g$	771	MPa
$\nu^r$	0.49	–
$\nu^g$	0.29	–
$R^{pg}$	10	MPa
$h$	0	MPa
$\Delta\theta$	30 (SEC) – 5 (CVS)	K
$\theta_t$	350 (SEC) – 344 (CVS)	K
$w$	0.2 (SEC) – 0.375 (CVS)	1/K
$c$	1	–
$c^p$	0	–

Table 1: Model parameters of the mechanical problem

257

258 Material properties listed in Table 1 are used for both cases. The software  
259 GetDP [44] was used to solve the fully coupled problem based on a total La-  
260 grangian formulation.

#### 261 4.1. Validation of the mechanical problem

262 Results of the thermo-mechanical model developed in [30] are reproduced.  
263 This model consisted of a temperature-dependent elasto-plastic model with a  
264 constant temperature field imposed for all Gauss points at any given time instant  
265  $t$ .

266 Results of the single element are reported in Figure 2 for a high-temperature  
267 fixing similar to the one used in [30]. The material is progressively deformed at  
268 400K, then cooled down to 200K while keeping constant the deformation. The  
269 material is then unloaded at 200K before re-heating it up to 400K to trigger the  
270 shape-recovery (see Test 1 in Fig. 6 of [30]). The results reported in Figure 2  
271 conform to those obtained in [30].

#### 272 4.2. New results of the coupled problem

273 The results of the coupled problem are presented below. A description of  
274 the mechanical, thermal and electromagnetic problems is followed by the pre-  
275 sentation of numerical results of the shape memory polymer. A best design can  
276 be obtained by choosing material properties for the thermal problem (thermal  
277 conductivity, mass density and heat capacity) that maintain a homogeneous  
278 temperature field in the stent, in order to avoid the appearance of regions with  
279 different phases during the recovery step. A non dimensionalization analysis of  
280 the thermal problem carried out in Section 4.2.2 facilitates this design. How-  
281 ever, the control of the temperature is complicated by the dependence of the  
282 mechanical stress on the temperature-dependent ratio of the glassy state  $z^g(\theta_L)$ .

283 The geometry of Figure 3 is used for the mechanical problem of the cylin-  
284 drical vascular stent.

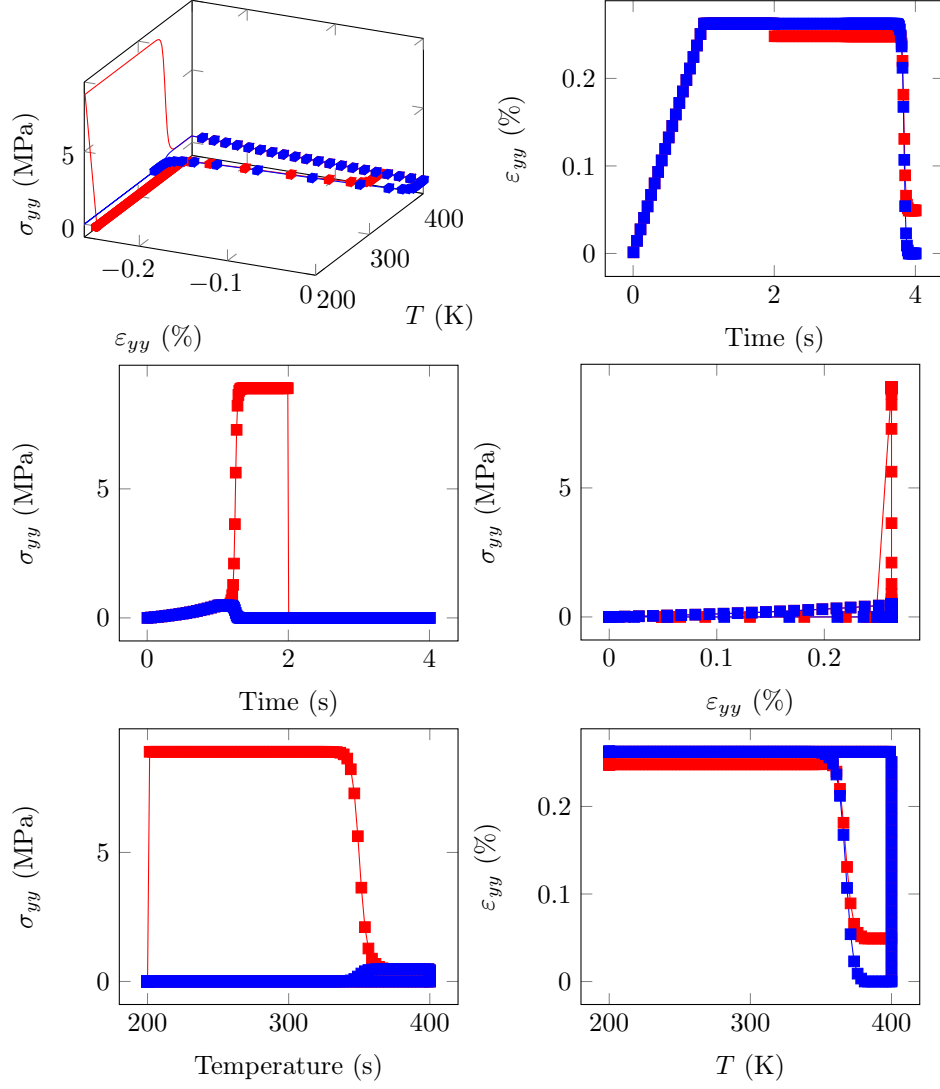


Figure 2: Results of the single element. Top-left: temperature–strain–stress curve. Top-right: strain versus time curve. Middle-left: stress versus time curve. Middle-right: strain versus stress curve. Bottom-left: temperature versus stress curve. Bottom-right: temperature versus strain curve. Blue curves correspond to the ideal case while red curves correspond to the non-ideal case.

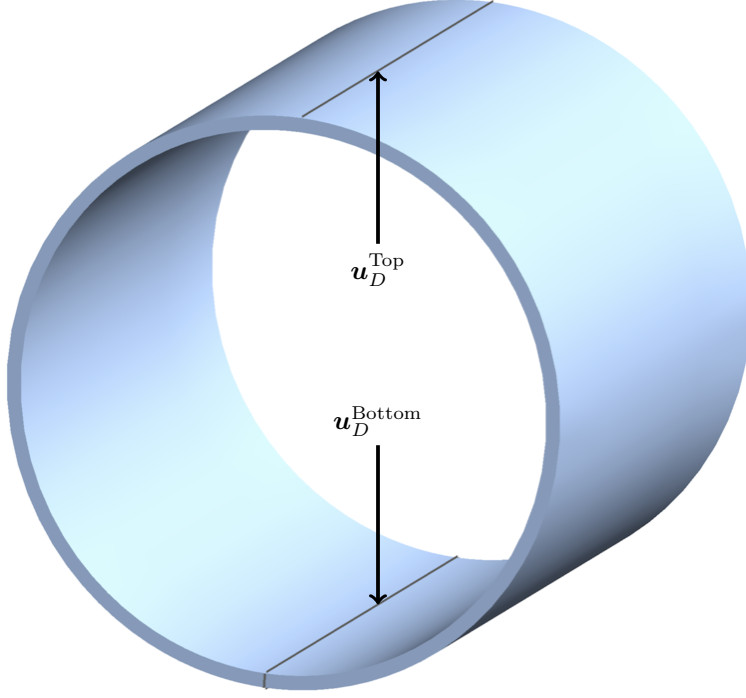


Figure 3: Dirichlet boundary conditions for the mechanical problem. Zero displacement  $\mathbf{u}_D^{\text{Bottom}}(t) = 0$  is imposed on the bottom section and a time-dependent displacement  $\mathbf{u}_D^{\text{Top}}(t)$  similar to the one used for Test 1 of Fig. 6 in [30] is imposed on the top line.

#### 285 4.2.1. Electromagnetic and thermal problems

286 We simulate the insertion of a vascular shape memory polymer stent in a vein  
 287 of the arm. The stent contains electric particles that can react to electromag-  
 288 netic source fields produced by a coil wrapped around the arm by producing heat  
 289 by the Joule effect. For the sake of simplicity, we consider the resulting shape  
 290 memory polymer composite to be homogeneous with homogenized macroscopic  
 291 material properties, thus ignoring the multiscale nature of the composite.

292 The mechanical problem is similar to the one in [30], with the temperature  
 293 field obtained by solving the thermal problem with the source generated by the  
 294 eddy current losses. In the following, we define the electromagnetic and the  
 295 thermal problems.

The temperature can be controlled by an electromagnetic field generated by

a coil crossed by a current denoted  $I_s(t)$ . For all problems studied herein, we consider a single frequency source

$$I_s(t) = I_0(t)(a + b \sin(\omega t)) = I_0(t)(a + b \sin(2\pi f t)), \quad (4.1)$$

where  $I_0(t)$  (A) is piecewise, linear, time-dependent amplitude of the electric current,  $\omega$  is the angular velocity and  $f$  the frequency of the signal. The design parameters for the electromagnetic and thermal problems are the amplitude of the current, the frequency and the material properties: the electric conductivity  $\sigma$  (S/m), the magnetic permeability  $\mu$  (H/m), the mass density  $\rho$ , the heat capacity  $c_p$  and the thermal conductivity  $\kappa$ . In all our applications, we consider frequencies small than 1000Hz,  $\sigma = 10^4$ S/m and  $\mu = \mu_0\mu_{\text{rel}}$  with  $\mu_{\text{rel}} = 20$ , which corresponds to the wavelength  $\lambda$  and skin depth  $\delta$ :

$$\lambda = \frac{c}{f} = \frac{1}{\sqrt{\mu\epsilon}f} \approx 300\text{km} \quad , \quad \delta = \sqrt{\frac{2}{\mu\sigma\omega}} \approx 40\text{mm}. \quad (4.2)$$

296 The wavelength is very large compared to the dimensions of the structure  
 297 (typically 20mm for the length and 1mm for the thickness) that the *quasistatic*  
 298 *assumption* can be made [45]. Likewise, the skin depth is large compared to  
 299 the dimensions of the stent that the eddy currents resulting from the reaction  
 300 field can be neglected. Figure 4 illustrates the geometry used for the coupled  
 301 problem.

To determine the magnetic induction source  $\mathbf{b}_s(t)$  for the electromagnetic problem, we consider a coil with a very large number of turns. The value of the magnetic field  $\mathbf{h}_s(t)$  and the magnetic induction  $\mathbf{b}_s(t)$  in the coil are homogeneous and given by [46]

$$\mathbf{h}_s(t) = h_s(t) \mathbf{e}_z = \frac{N}{L} I_s(t) \mathbf{e}_z, \quad \mathbf{b}_s(t) = b_s(t) \mathbf{e}_z = \mu \mathbf{h}_s(t) = \mu \frac{N}{L} I_s(t) \mathbf{e}_z \quad (4.3)$$

where  $N$  is the number of turns,  $L$  the length of the coil,  $\mu$  the magnetic permeability of the material and  $\mathbf{e}_z$  the direction oriented along the axis of the coil. From the Gauss magnetic law  $\text{div} \mathbf{b}_s = 0$ , a source vector potential  $\mathbf{a}_s(t)$  can be derived from the magnetic induction  $\mathbf{b}_s(t)$  as  $\mathbf{b}_s(t) = \text{curl} \mathbf{a}_s(t)$ . In the computational domain of the stent, a possible vector potential that satisfies this

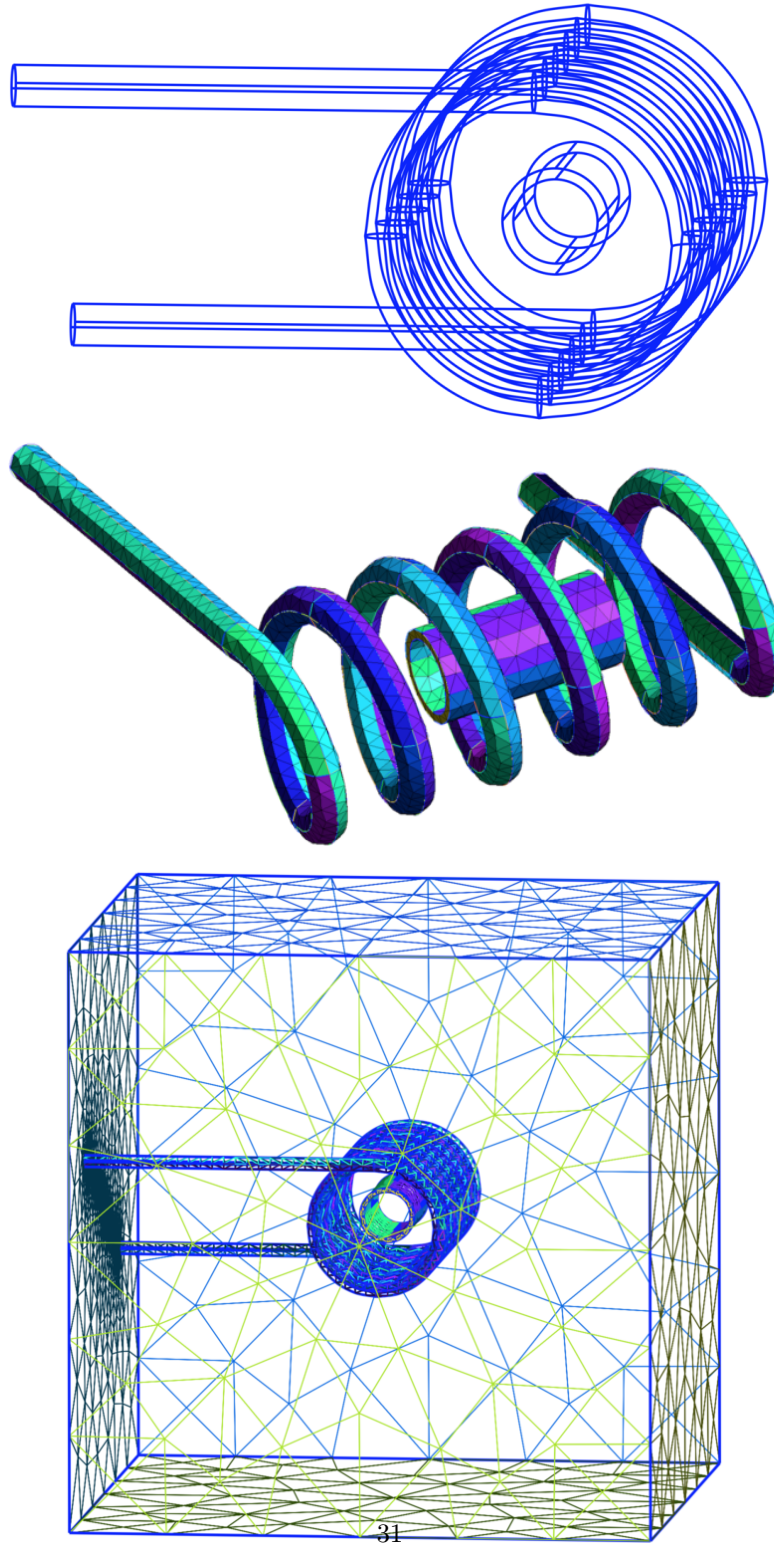


Figure 4: Geometry and mesh used for the coupled problem. Top: The cylindrical cardiovascular stent surrounded by an exciting coil. Middle: Mesh of the stent and the coil. Bottom: Mesh of the stent, the coil and the surrounding air. The enclosing box is used to bound the computational domain for the electromagnetic problem assumed to be unbounded.

equality and is symmetric with respect to the undeformed geometry of the stent is

$$\mathbf{a}_s(x, y, t) = 0.5 \mathbf{b}_s(t)(-y, x, 0) = 0.5 \mu \frac{N}{L} I_s(t)(-y, x, 0) \quad (4.4)$$

with  $x = X + u_x$  and  $y = Y + u_y$  where  $X$  and  $Y$  are the coordinates expressed in the undeformed configuration and  $u_x$  and  $u_y$  are components of the displacement  $\mathbf{u} = (u_x, u_y, u_z)$ . From (4.3) and (4.4), it can be noted that the magnetic field  $\mathbf{h}_s(t)$  and the magnetic induction  $\mathbf{b}_s(t)$  in the coil do not depend on spatial coordinates whereas the vector potential  $\mathbf{a}_s(t)$  depends on spatial coordinates  $x$  and  $y$ . This vector potential is a one differential form that can be transformed as  $\mathcal{A}_s = \mathbf{F}^T \mathbf{a}_s$  thus leading to the source in (2.15).

Table 2 contains model parameters of the electromagnetic and thermal problems.

Symbol	Value	Unit
$I_0(t)$	electric current waveform	A
$f$	1000	Hz
$\sigma$	$10^4$	S/m
$\mu_r$	20	—
$\rho$	270	kg m <sup>-3</sup>
$c_p$	10	kg m <sup>2</sup> K <sup>-1</sup> s <sup>-2</sup>
$k$	237	W m <sup>-1</sup> K <sup>-1</sup>
$h$	500	W m <sup>-2</sup> K <sup>-1</sup>
$N$	1000	—
$L$	1	m

Table 2: Model parameters of the electromagnetic and thermal problems

311

Defining the thermal problem resulting from the deployment of the actual stent is challenging. Though it is easy to control the temperature of the device during the first three stages (*loading* at high temperature, *cooling* followed by



unloading/insertion of the stent) most of which are done outside the human body, the last step, the *recovery*, necessitates controlling the temperature using electromagnetic fields. In this paper, we simulate the control of the entire deployment process using the electromagnetic fields.

During the last step, different modes of heat exchange can be considered: (1) heat conduction in the stent, at the interface of the stent and the surrounding tissue and in the tissue itself and (2) forced convection at part of the boundary of surface of the stent in contact with the blood flowing in the vein. The surface of the stent in contact with the tissue/blood varies during the process of recovery and its detection would necessitate consideration of contact mechanics. For the sake of simplicity, we only consider forced convection.

Finally, thanks to the assumptions made of the electromagnetic and thermal problems, all three problems can only be solved on the computational domain of the stent thus neglecting the surrounding environment.

#### 4.2.2. Results of the coupled problems

Results of the coupled problem are herein reported. As mentioned earlier, the main difference between this section and section 4.1 lies in the use of a temperature field obtained by solving the heat equation on a moving domain with the source obtained by solving the electromagnetic problem instead of a priori imposing a temperature field at each time instant  $t$ .

Figures 5 and 6 show the displacement  $\mathbf{u}$ , the current density  $\mathbf{j}$ , Joule losses and the temperature  $T$  at the instances  $t = 4.78125 \times 10^{-3}\text{s}$  and  $t = 4.84375 \times 10^{-3}\text{s}$ . This can play an important role in the design of the stent, especially for the computation of the temperature. Indeed, the high dependency of the ratio of the glassy states on the temperature  $z^g(\theta_L)$  necessitates selecting electromagnetic and thermal loadings as well as thermal material properties that allow for a quick diffusion of the heat sources throughout the stent, to avoid inhomogeneities of temperature that would cause different regions of the stent to be in different phases (rubbery/glassy) during the recovery step. Another issue concerns the use of the Newton–Raphson method to solve the

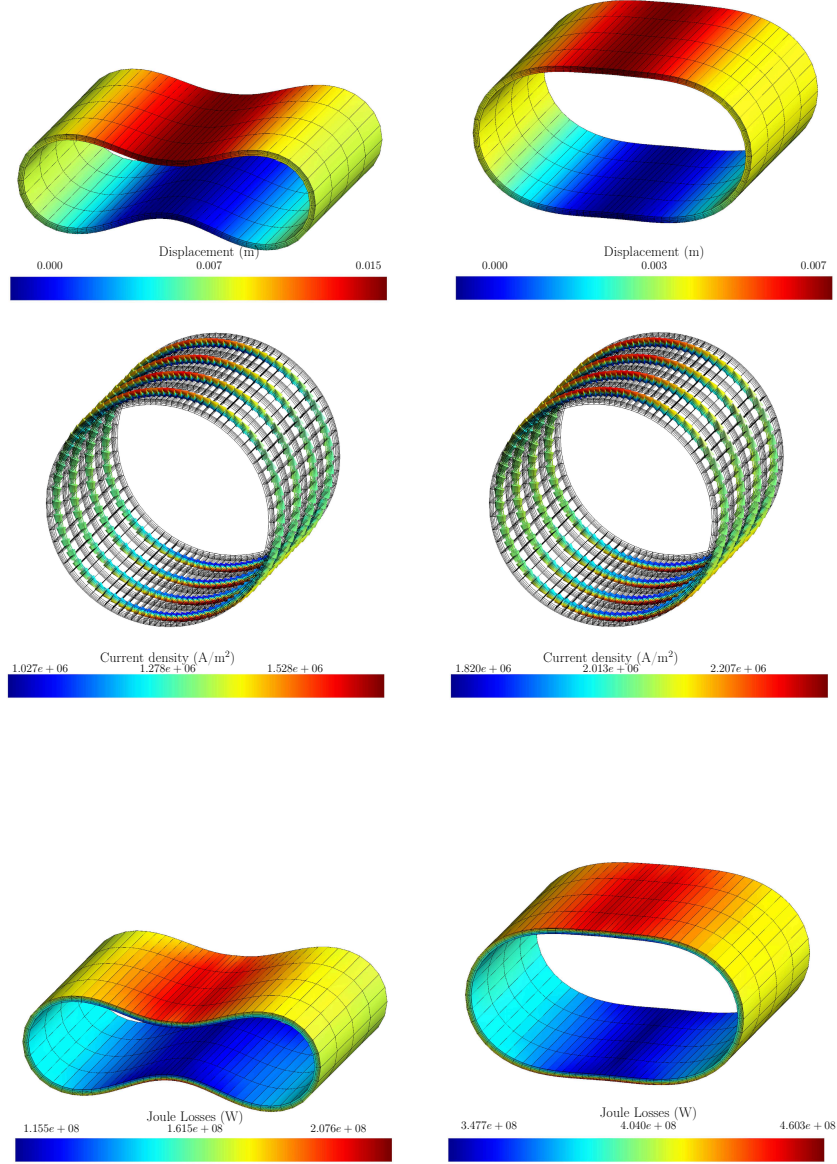


Figure 5: Physical fields during the recovery. The left images correspond to  $t = 4.78125 \times 10^{-3} \text{s}$  and the right images correspond to  $t = 4.84375 \times 10^{-3} \text{s}$ . Top : displacement  $\mathbf{u}$ , middle : current density  $\mathcal{J}$ , bottom : Joule losses  $w_L$ .

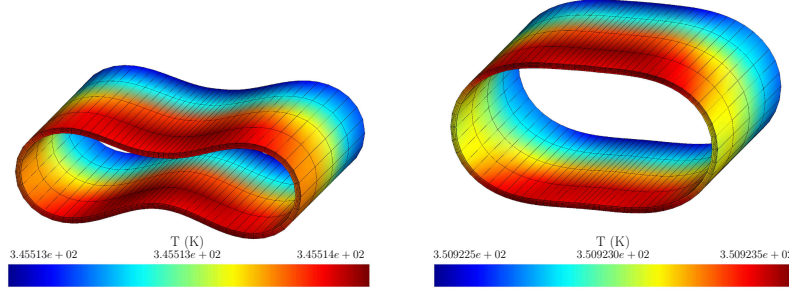


Figure 6: Temperature at  $t = 4.78125 \times 10^{-3}$ s (left) and  $t = 4.84375 \times 10^{-3}$ s (right).

nonlinear coupled problem. Considerably large and inhomogeneous increments of temperature computed especially during the first nonlinear iterations of the Newton–Raphson scheme may lead to inhomogeneities of temperature and cause slow convergence in the recovery process.

To avoid inhomogeneities of temperature in the recovery step, we developed the following normalization process, which makes the problem well conditioned.

The process starts with the linearized version of the *heat equation* (3.34):

$$\rho_L c_p \frac{\partial \theta_L}{\partial t} + \text{Div}_X [\kappa_L \mathbf{Grad}_X \theta_L] = -w_L(\phi, \theta_L, \mathbf{u}). \quad (4.5)$$

A new coordinate system  $(\tau, \boldsymbol{\eta})$  is introduced as:

$$\begin{aligned} t = T_c \tau, \quad dt = T_c d\tau, \quad \frac{\partial(\cdot)}{\partial t} &= \frac{1}{T_c} \frac{\partial(\cdot)}{\partial \tau}, \\ X_i = L_c \eta_i, \quad dX_i = L_c d\eta_i, \quad \frac{\partial(\cdot)}{\partial X_i} &= \frac{1}{L_c} \frac{\partial(\cdot)}{\partial \eta_i}, \quad \theta_L = \theta_c \bar{\theta}_L \end{aligned} \quad (4.6)$$

where  $\bar{\theta}$ ,  $T_c$ ,  $L_c$ ,  $\tau$ , and  $\eta_i$  are the characteristic temperature, the characteristic time, the characteristic length, the dimensionless temporal and spatial coordinates, respectively. The derivatives in (4.5) are transformed as:

$$\begin{aligned} \frac{\partial \theta_L}{\partial t} &= \frac{1}{T_c} \frac{\partial(\theta_c \bar{\theta}_L)}{\partial \tau} = \frac{\theta_c}{T_c} \frac{\partial \bar{\theta}_L}{\partial \tau}, \quad \frac{\partial \theta_L}{\partial X_i} = \frac{1}{L_c} \frac{\partial(\theta_c \bar{\theta}_L)}{\partial \eta_i} = \frac{\theta_c}{L_c} \frac{\partial \bar{\theta}_L}{\partial \eta_i}, \\ \frac{\partial^2 \theta_L}{\partial X_i^2} &= \frac{1}{L_c^2} \frac{\partial \left( \frac{\partial \theta_L}{\partial x_i} \right)}{\partial \eta_i} = \frac{\theta_c}{L_c^2} \frac{\partial^2 \bar{\theta}_L}{\partial \eta_i^2} \end{aligned} \quad (4.7)$$

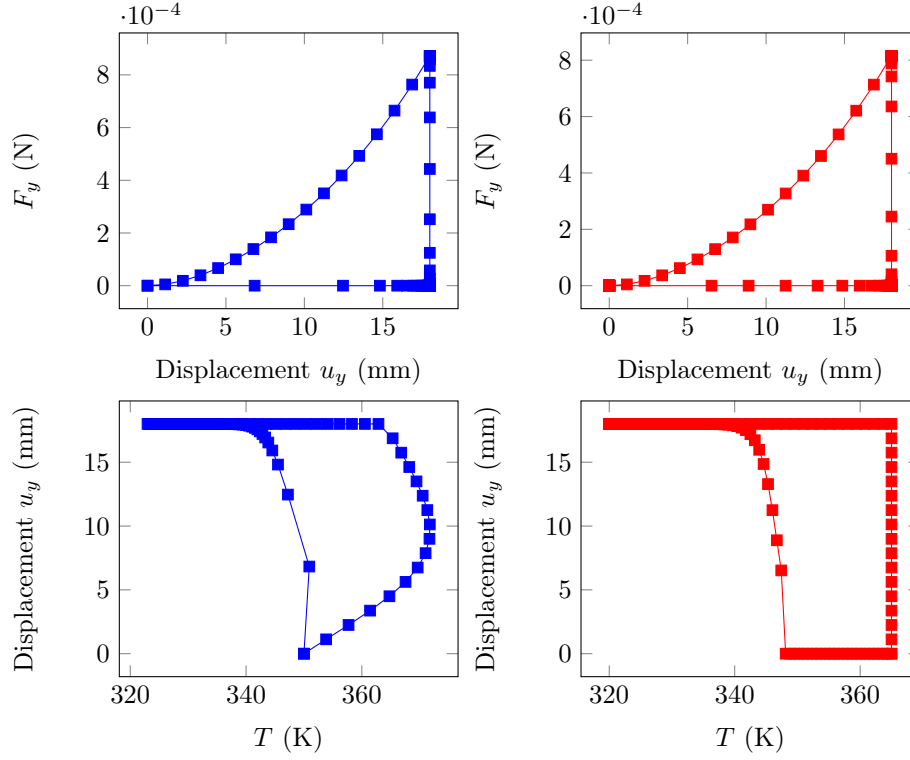


Figure 7: Results of the coupled problem. Top : Force versus displacement curves. Computed temperature (left) and imposed temperature (right). Bottom: Displacement versus temperature curves. Computed temperature (left) and imposed temperature (right).

which leads to the *dimensionless heat equation*:

$$\frac{\partial \bar{\theta}_L}{\partial \tau} + \frac{T_c \bar{\kappa}_L}{\rho_L c_p L_c^2} \text{Div}_\eta [\mathbf{Grad}_\eta \bar{\theta}_L] = -\frac{T_c}{\rho_L c_p L_c^2} \bar{w}_L(\bar{\phi}, \bar{\theta}_L, \bar{\mathbf{u}}) \quad (4.8)$$

where the thermal conductivity was assumed constant and barred quantities are defined in the new coordinate system. For the first two terms to be of the same order of magnitude, i.e., for the temperature to have enough time to diffuse in the stent, the material properties must be chosen such that

$$T_c = \frac{\rho_L c_p L_c^2}{\bar{\kappa}_L}. \quad (4.9)$$

351 Results of the coupled problem are reported in Figures 7-8 for a stent with  
 352 the high-temperature fixing and slightly different material properties as those

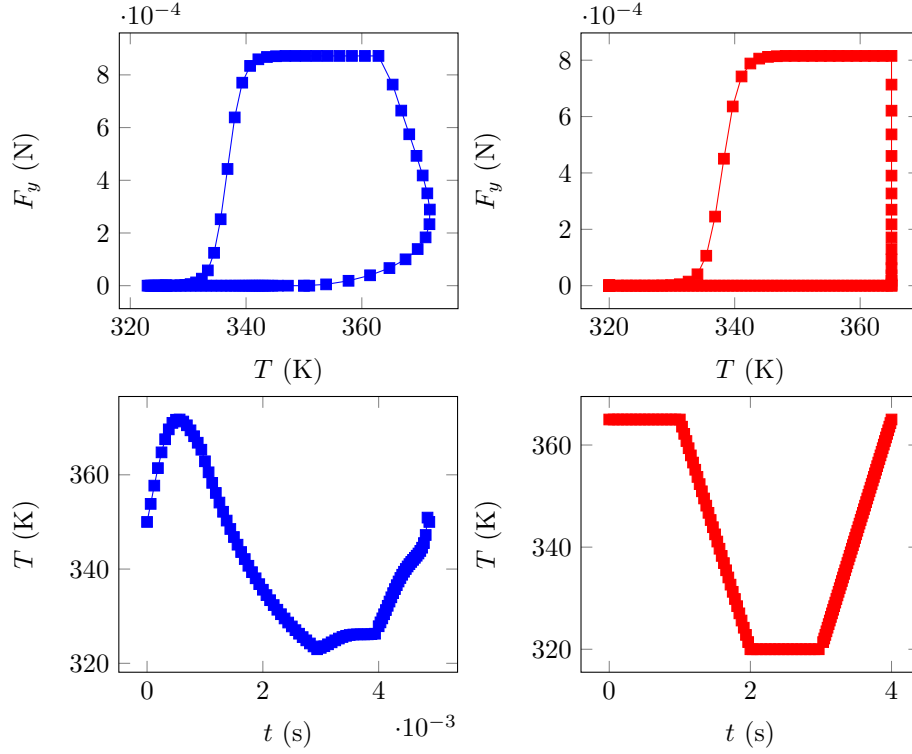


Figure 8: Results of the coupled problem. Top : Force versus temperature curves. Computed temperature (left) and imposed temperature (right). Bottom : Temperature versus time curves. Computed temperature (left) and imposed temperature (right).

353 reported in [30]. In the case of the imposed temperature, the material is pro-  
 354 gressively deformed at 350K, then cooled down to 320K while the deformation is  
 355 maintained constant, then unloaded at 320K, and finally re-heated up to 350K  
 356 to trigger shape-recovery. We mimick the same trajectory of the temperature by  
 357 changing material properties, the frequency and the amplitude of the excitation  
 358 source. Results of the coupled problem are different from the ones obtained  
 359 with the imposed temperature. An optimal control of the temperature using  
 360 the source current  $I_s(t)$  and the geometry of the coil as control parameters can  
 361 allow to prescribe a temperature trajectory convenient for surgical purposes.

## 362 5. Conclusions

363 In this paper, the deployment of a vascular shape memory polymer stent  
364 in a vein of an arm is simulated. The temperature field used in the thermo-  
365 mechanical model of the stent is controlled by solving for electromagnetic fields  
366 generated by a coil wrapped around the arm. The controllability of the tem-  
367 perature depends on the choice of the electromagnetic source field determined  
368 by the amplitude and the excitation frequency of the current flowing through  
369 the coil, and on the material properties used for the thermal problem. An ini-  
370 tial design of the stent which allows for the diffusion of heat and leads to a  
371 homogeneous distribution of temperature during the recovery step is proposed.  
372 The optimal control of the temperature of the devices can further be carried  
373 out, thus allowing the device to follow a prescribed temperature trajectory that  
374 might be convenient for surgical purposes.

## 375 Acknowledgments

376 The authors would like to thank Dr. Elisa Boatti at Georgia Institute of  
377 Technology, Prof. Ludovic Noels and Miguel Pareja Muñoz at the University of  
378 Liège for fruitful discussions on mechanical models of shape memory polymers.  
379 They would also like to thank Prof. Christophe Geuzaine at the University of  
380 Liège for discussions about the implementation in GetDP. The first author is  
381 particularly indebted to Dr. François Henrotte at the University of Liège for the  
382 discussions on electromagnetic formulations under large deformations. During  
383 the time the research was carried out, Innocent Niyonzima was a postdoctoral  
384 Fellow with the Belgian American Educational Foundation (BAEF). He is also  
385 partially supported by an excellence grant from Wallonie-Bruxelles International  
386 (WBI).

## 387 References

- 388 [1] An introduction to biomaterials, [https://www.uweb.engr.washington.](https://www.uweb.engr.washington.edu/research/tutorials/introbiomat.html)  
389 [edu/research/tutorials/introbiomat.html](https://www.uweb.engr.washington.edu/research/tutorials/introbiomat.html), accessed: 2017-12-22.

- 390 [2] S. K. Bhatia, Biomaterials for clinical applications, Springer Science &  
391 Business Media, 2010.
- 392 [3] H. R. Rezaie, L. Bakhtiari, A. Öchsner, Biomaterials and their applications,  
393 Springer, 2015.
- 394 [4] W. M. Huang, B. Yang, Y. Q. Fu, Polyurethane shape memory polymers,  
395 CRC Press, 2011.
- 396 [5] W. Small, P. R. Buckley, T. S. Wilson, W. J. Bennett, J. Hartman, D. Sa-  
397 loner, D. J. Maitland, Shape memory polymer stent with expandable foam:  
398 a new concept for endovascular embolization of fusiform aneurysms, IEEE  
399 Transactions on Biomedical Engineering 54 (6) (2007) 1157–1160.
- 400 [6] D. J. Maitland, W. Small, J. M. Ortega, P. R. Buckley, J. Rodriguez,  
401 J. Hartman, T. S. Wilson, Prototype laser-activated shape memory polymer  
402 foam device for embolic treatment of aneurysms, Journal of biomedical  
403 optics 12 (3) (2007) 030504–030504.
- 404 [7] C. M. Yakacki, R. Shandas, C. Lanning, B. Rech, A. Eckstein, K. Gall, Un-  
405 constrained recovery characterization of shape-memory polymer networks  
406 for cardiovascular applications, Biomaterials 28 (14) (2007) 2255–2263.
- 407 [8] G. M. Baer, T. S. Wilson, W. Small, J. Hartman, W. J. Bennett, D. L.  
408 Matthews, D. J. Maitland, Thermomechanical properties, collapse pressure,  
409 and expansion of shape memory polymer neurovascular stent prototypes,  
410 Journal of Biomedical Materials Research Part B: Applied Biomaterials  
411 90 (1) (2009) 421–429.
- 412 [9] S. H. Ajili, N. G. Ebrahimi, M. Soleimani, Polyurethane/polycaprolactane  
413 blend with shape memory effect as a proposed material for cardiovascular  
414 implants, Acta biomaterialia 5 (5) (2009) 1519–1530.
- 415 [10] L. Yahia, Shape memory polymers for biomedical applications, Elsevier,  
416 2015.

- 417 [11] C. Wischke, A. T. Neffe, S. Steuer, A. Lendlein, Comparing techniques for  
418 drug loading of shape-memory polymer networks—effect on their functional-  
419 ities, *European Journal of Pharmaceutical Sciences* 41 (1) (2010) 136–147.
- 420 [12] K. Nagahama, Y. Ueda, T. Ouchi, Y. Ohya, Biodegradable shape-memory  
421 polymers exhibiting sharp thermal transitions and controlled drug release,  
422 *Biomacromolecules* 10 (7) (2009) 1789–1794.
- 423 [13] J. Fish, W. Chen, Modeling and simulation of piezocomposites, *Computer*  
424 *methods in applied mechanics and engineering* 192 (28-30) (2003) 3211–  
425 3232.
- 426 [14] M. Elhadrouz, T. B. Zineb, E. Patoor, Finite element analysis of a multi-  
427 layer piezoelectric actuator taking into account the ferroelectric and ferroe-  
428 lastic behaviors, *International journal of engineering science* 44 (15) (2006)  
429 996–1006.
- 430 [15] P. I. Anderson, A. J. Moses, H. J. Stanbury, Assessment of the stress sensi-  
431 tivity of magnetostriction in grain-oriented silicon steel, *IEEE transactions*  
432 *on magnetics* 43 (8) (2007) 3467–3476.
- 433 [16] M. Khalaquzzaman, B. Xu, S. Ricker, R. Müller, Computational homoge-  
434 nization of piezoelectric materials using  $FE^2$  to determine configurational  
435 forces, *Technische Mechanik* 32 (1) (2012) 21–37.
- 436 [17] S. Kuznetsov, J. Fish, Mathematical homogenization theory for electroac-  
437 tive continuum, *International Journal for Numerical Methods in Engineer-*  
438 *ing* 91 (11) (2012) 1199–1226.
- 439 [18] O. Perevertov, J. Thielsch, R. Schäfer, Effect of applied tensile stress on the  
440 hysteresis curve and magnetic domain structure of grain-oriented transverse  
441 Fe-3% Si steel, *Journal of Magnetism and Magnetic Materials* 385 (2015)  
442 358–367.
- 443 [19] P. L. Bishay, S. N. Atluri, Computational Piezo-Grains (CPGs) for a  
444 highly-efficient micromechanical modeling of heterogeneous piezoelectric–



- 445 piezomagnetic composites, *European Journal of Mechanics-A/Solids* 53  
446 (2015) 311–328.
- 447 [20] A. C. Eringen, G. A. Maugin, *Electrodynamics of continua I: foundations*  
448 *and solid media*, Springer Science & Business Media, 2012.
- 449 [21] Y.-H. Pao, Electromagnetic forces in deformable continua, in: *Mechanics*  
450 *today*, Vol. 4, 1978, pp. 209–305.
- 451 [22] R. Ogden, Incremental elastic motions superimposed on a finite deforma-  
452 tion in the presence of an electromagnetic field, *International Journal of*  
453 *Non-Linear Mechanics* 44 (5) (2009) 570–580.
- 454 [23] P. Saxena, On the general governing equations of electromagnetic acoustic  
455 transducers, *Archive of Mechanical Engineering* 60 (2) (2013) 231–246.
- 456 [24] M. Stiemer, J. Unger, B. Svendsen, H. Blum, An arbitrary Lagrangian Eule-  
457 rian approach to the three-dimensional simulation of electromagnetic form-  
458 ing, *Computer Methods in Applied Mechanics and Engineering* 198 (17)  
459 (2009) 1535–1547.
- 460 [25] B. E. Abali, A. F. Queiruga, Theory and computation of electromagnetic  
461 fields and thermomechanical structure interaction for systems undergoing  
462 large deformations, <https://arxiv.org/abs/1803.10551>, accessed: 2018-  
463 12-20.
- 464 [26] G. Ethiraj, C. Miehe, Multiplicative magneto-elasticity of magnetosensitive  
465 polymers incorporating micromechanically-based network kernels, *Interna-*  
466 *tional Journal of Engineering Science* 102 (2016) 93–119.
- 467 [27] C. Miehe, D. Vallicotti, S. Teichtmeister, Homogenization and multiscale  
468 stability analysis in finite magneto-electro-elasticity. Application to soft  
469 matter EE, ME and MEE composites, *Computer Methods in Applied Me-*  
470 *chanics and Engineering* 300 (2016) 294–346.

- [28] A. Bayat, F. Gordaninejad, Characteristic volume element for randomly particulate magnetoactive composites, *Journal of Engineering Materials and Technology* 140 (1) (2018) 011003.
- [29] L. Homsí, L. Noels, A discontinuous Galerkin method for non-linear electro-thermo-mechanical problems: application to shape memory composite materials, *Meccanica* (2017) 1–45.
- [30] E. Boatti, G. Scalet, F. Auricchio, A three-dimensional finite-strain phenomenological model for shape-memory polymers: Formulation, numerical simulations, and comparison with experimental data, *International Journal of Plasticity* 83 (2016) 153–177.
- [31] P. Wriggers, *Nonlinear finite element methods*, Springer Science & Business Media, 2008.
- [32] P. L. Penfield Jr, L. Chu, H. A. Haus, *Electrodynamics of moving media*, Tech. rep., Research Laboratory of Electronics (RLE) at the Massachusetts Institute of Technology (MIT) (1963).
- [33] R. M. Fano, L. J. Chu, R. B. Adler, *Electromagnetic fields, energy, and forces*, MIT Press, 1968.
- [34] J. D. Jackson, *Classical Electrodynamics*, 3rd Edition, Wiley, 1998.
- [35] A. B. de Castro, D. Gómez, P. Salgado, *Mathematical models and numerical simulation in electromagnetism*, Vol. 74, Springer, 2014.
- [36] J. C. Simo, T. J. Hughes, *Computational inelasticity*, Vol. 7, Springer Science & Business Media, 2006.
- [37] T. Belytschko, W. K. Liu, B. Moran, K. Elkhodary, *Nonlinear finite elements for continua and structures*, John Wiley & Sons, 2013.
- [38] R. Hiptmair, O. Sterz, Current and voltage excitations for the eddy current model, *International Journal of Numerical Modelling: Electronic Networks, Devices and Fields* 18 (1) (2005) 1–21.

- 498 [39] A. Bossavit, Computational Electromagnetism. Variational Formulations,  
499 Complementarity, Edge Elements, Academic Press, 1998.
- 500 [40] R. Scorretti, R. V. Sabariego, L. Morel, C. Geuzaine, N. Burais, L. Nicolas,  
501 Computation of induced fields into the human body by dual finite element  
502 formulations, IEEE Transactions on Magnetism 48 (2) (2012) 783–786.
- 503 [41] F. Bachinger, U. Langer, J. Schöberl, Numerical analysis of nonlinear mul-  
504 tiharmonic eddy current problems, Numerische Mathematik 100 (4) (2005)  
505 593–616.
- 506 [42] T. J. Hughes, The finite element method: linear static and dynamic finite  
507 element analysis, Courier Corporation, 2012.
- 508 [43] J. Fish, T. Belytschko, A first course in finite elements, John Wiley, 2007.
- 509 [44] P. Dular, C. Geuzaine, F. Henrotte, W. Legros, A general environment for  
510 the treatment of discrete problems and its application to the finite element  
511 method, IEEE Transactions on Magnetism 34 (5) (1998) 3395–3398.
- 512 [45] A. A. Rodríguez, A. Valli, Eddy Current Approximation of Maxwell Equa-  
513 tions: Theory, Algorithms and Applications, Vol. 4, Springer Science &  
514 Business Media, 2010.
- 515 [46] The electromagnetic fields generated by a long solenoid, [http://](http://hyperphysics.phy-astr.gsu.edu/hbase/magnetic/solenoid.html)  
516 [hyperphysics.phy-astr.gsu.edu/hbase/magnetic/solenoid.html](http://hyperphysics.phy-astr.gsu.edu/hbase/magnetic/solenoid.html), ac-  
517 cessed: 2018-06-04.